The ice front as a topographic barrier for ocean heat transport

Nadine Steiger

Thesis for the degree of Philosophiae Doctor (PhD)
University of Bergen, Norway
2021

UNIVERSITY OF BERGEN

The ice front as a topographic barrier for ocean heat transport

Nadine Steiger

Thesis for the degree of Philosophiae Doctor (PhD)
at the University of Bergen

Date of defense: 28.06.2021

Year: 2021

Title: The ice front as a topographic barrier for ocean heat transport

Name: Nadine Steiger

Print: Skipnes Kommunikasjon / University of Bergen

Scientific environment

The research for this dissertation was carried out at the Geophysical Institute, University of Bergen and the Bjerknes Center for Climate Research (BCCR). Part of the work (equivalent of 5 months) was carried out at the Nansen Environmental and Remote Sensing Center (NERSC). The work was part of the project "Topographic Barriers controlling warm water inflow and Antarctic Ice Shelf Melting" (TOBACO) funded by the Norwegian Research Council (grant number 267660) and let by my supervisor Elin Darelius. My co-supervisor Anna Wåhlin kindly hosted me for two two-month research stays at the University of Gothenborg. I was enrolled in the Norwegian Research School on Changing Climates in the coupled Earth System (CHESS), which provided many relevant courses. The summer school "Fluid Dynamics of Sustainability and the Environment" (FDSE) was funded by the Meltzer foundation. The experiments at the Coriolis platform in Grenoble, France were supported by the European Unions H2020 program through the grant to Hydralab-plus, contract number 654110. The computational resources for the numerical modelling were provided through the Notur grants NN9481K and NS9481K. In-between the work for this dissertation, but unrelated, I got the opportunity to join an Antarctic cruise with the Norwegian Polar Institute to Dronning Maud Land with RV Kronprins Håkon.

Acknowledgements

I have been excited about Antarctica already a long time ago. Thank you Elin, for giving me this great opportunity to work on such an interesting project with laboratory experiments, modelling, observations and the chance to join a cruise to the Southern Ocean. It has been great to work with you, to get all your help, your insights into dynamical oceanography and your encouragement to do some fun-stuff related to outreach. Anna, thank you for hosting me in Gothenborg, for helping me with the theory, for making me co-author of a Nature-paper (I still think this is pretty cool!), but also for asking critical questions about my modelling work. Toshi, thank you for helping me with MITgcm, it was incredibly helpful to have you visiting us in Bergen. Another thanks goes to Annette for hosting me at NERSC and for making me feel welcome in the group.

Next, I want to thank everyone who was involved in the lab experiments, especially Joel for helping with the data processing and Samuel and Thomas for working hard to make the experiments work. Thank you Mirjam for your infectious excitement about basically anything and for all your extremely inspiring outreach work (I do love the article in Frontiers for Young Minds). Another thanks to Ryan for all your useful and detailed explanations regarding momentum/ vorticity budgets and other MITgcm-stuff. Thanks for an enjoyable stay in Cambridge, I met a lot of great people there and got a lot of input in only a few days. Another thanks goes to Karen for sharing all your knowledge about the Amundsen Sea and various great discussions. Vår, thanks for your helpful feedback on my texts and many discussions on confusing processes. Another thanks to Kjersti for always having good advises and an open ear. Altogether, I feel very fortunate that I could be part of a great scientific environment and a supportive PhD community at GFI and Bjeknes that made it enjoyable to go to work.

I am grateful to have amazing friends here in Bergen and at home who filled my PhD period with fun, laughter and great memories. Thank you Astrid for having been such a good friend since my very first day in Bergen. The same counts for Morven, thanks for nice trips (EGU/ Olomouc), fun parties and for being very inspiring. I want to thank all the climbing (and much more than only climbing)-crew (Sonja, Anaïs, Zoe, Nora, Fran, Augustin, AK, Danielle, Jonathan) for hours and hours in the chalky cave, especially after long hours in the office. Thank you all also for the skiing, climbing and surfing adventures, runs, dinners, cooking, baking, parties, bonfires etc... To the Monday dinner crew: I don't remember when I had to laugh as much as with you! Barbara, Caro, Carina, Andreas: Ihr seid unersetzlich! Rebecca, ich bin echt froh dich zu kennen und dass wir es einfach immer und überall schaffen uns zu treffen, selbst in PA!

This is to my family: Vielen Dank für eure unendliche Unterstützung, euer Interesse an Antarktisforschung, lange Telefonate und eure positive Einstellung! Last but not least, the biggest thanks is to Lander for being the best home-office buddy, for helping me with the writing, for distracting me from work for many unforgettable skiing-running-climbing-surfing-cycling-camping-Maxiing-trips, and for always making sure I fall asleep with a big smile in my face.

Nadine Steiger
Bergen, March 29, 2021

Abstract

Antarctic ice shelves are the link between the Southern Ocean and the Antarctic Ice Sheet. The floating ice shelves restrain the seaward flow of the grounded ice, which is balanced by iceberg calving and ocean-induced basal melting. An increase in oceanic heat flux towards the West Antarctic ice shelves during the last decades has caused the ice shelves to thin. Nevertheless, the observed melt rates are lower than expected from the oceanic heat available on the continental shelf, suggesting that not all the heat is used to melt the ice shelves. Ice shelves extend several hundred meters into the ocean and terminate with a vertical wall, the ice front, that poses a topographic barrier to the ocean heat transport towards the sub-ice shelf cavities. Little is known about the influence of the discontinuity in water column thickness on the southward currents that transport warm and dense Circumpolar Deep Water from north of the continental shelf towards the ice shelf cavities. This thesis improves our understanding of the ocean dynamics and the drivers of heat transport variability in the vicinity of the ice front, based on mooring observations in front of the Getz Ice Shelf in West Antarctica, laboratory experiments, and idealized numerical modelling.

From the mooring observations, we infer in Paper I that only a small fraction of the southward heat transport eventually reaches the Getz Ice Shelf cavity, due to the different response of the barotropic (depth-constant) and the baroclinic (depth-varying) components of the current to the ice front. The barotropic component is blocked and deflected at the ice front; only the baroclinic, bottom-intensified component enters the ice shelf cavity. Results from laboratory experiments on a rotating platform support these observations. The experiments show that the barotropic current follows lines of constant water column thickness and turns at the ice front, while the baroclinic, dense current follows lines of constant bed topography and enters the cavity without being influenced by the ice front.

The heat transport towards the Getz Ice Shelf cavity is additionally reduced by intermittent deepening of cold and fresh Winter Water towards the bottom, disrupting the southward flow of the warm Circumpolar Deep Water. We show in Paper II that the deepening of the Winter Water is triggered by easterly winds and coastal Ekman downwelling in about 100 km distance from the moorings. The signal appears to propagate westward towards the mooring site as a coastal trapped wave. While the cold Winter Water deepens at the ice front, the velocities at depth do no longer align with the bathymetry directed towards the cavity, but flow parallel to the ice front. The number of these events during each winter and the consequent reduction in heat transport depends on the number of strong wind events and the pre-conditioning of the water column.

In Paper III, we investigate the dynamics of an externally forced barotropic current colliding with an ice front, using idealized numerical model simulations. When the barotropic current reaches the ice front, most of the flow is deflected, in agreement with the observations in Paper I and the theory of geostrophy. A fraction of the barotropic flow over a sloping bottom can enter the ice shelf cavity depending on the ice shelf thickness and background stratification. In a non-stratified ocean, the change in water column thickness largely determines the volume flux into the cavity. The flow can pass the discontinuity because of ageostrophic processes and large vertical velocities as the water column squeezes into the cavity. The part of the flow that is blocked develops a narrow and fast current parallel to the ice front that causes high melt rates in the frontal region. In a stratified ocean, in contrast, vertical velocities at the ice front are suppressed, and the upper water column is unable to flow under the ice shelf. Consequently, most of the flow is blocked by the ice front.

The three papers in this thesis show that the vertical front of Antarctic ice shelves affect the transport of ocean heat into the underlying cavities. The deflection of ocean heat transport at the ice front is relevant for the basal melting of ice shelves. The amount of ocean heat delivered to the base of the ice shelves depends on the relative contribution of the barotropic and the baroclinic components, the vertical density structure of the water column, and the geometry of the ice shelf. Surface winds and sea ice growth modify the vertical structure of the water column and drive the variability in heat transport into the ice shelf cavity.

Outline

This thesis consists of an introductory part and three scientific papers. The introduction starts with a motivation of the study (Chapter 1), followed by background information (Chapter 2). The background includes a description of the region of interest—the Amundsen Sea and the Getz Ice Shelf—, an overview of relevant oceanographic concepts and the ocean heat transport onto the continental shelf and into the cavity, and finally processes involved in ice shelf basal melting. Then, I describe the objectives of this study (Chapter 3) and the data and methods used in the three papers (Chapter 4). The papers are summarized in Chapter 5 followed by concluding remarks (Chapter 6).

The three papers contained in this thesis are:

I Wåhlin, A.K., Steiger, N., Darelius, E., Assmann, K.M., Glessmer, M.S., Ha, H.K., Herraiz-Borreguero, L., Heuzé, C., Jenkins, A., Kim, T.W., Mazur, A.K., Sommeria, J., Viboud, S.(2020), *Ice front blocking of ocean heat transport to an Antarctic ice shelf*, Nature **578**

II Steiger, N., Darelius, E., Wåhlin, A. K., Assmann, K. M. *Intermittent reduction in ocean heat transport into the Getz Ice Shelf cavity during strong wind events* (submitted to Geophysical Research Letters)

III Steiger, N., Darelius, E., Kimura, S., Patmore, R. D., Wåhlin, A. K. *The dynamics of a barotropic current at an ice front*, (in review in Journal of Physical Oceanography)

My main responsibilities in Paper I are related to the laboratory experiments, including the conduction and documentation of the experiments together with other authors, as well as calibration, processing and analysis of the experimental data. I produced the text and the Figures related to the experiments (Fig. 4, Extended Data Fig. 9 and parts of Extended Data Fig. 7). Additionally, I made Fig. 1 and contributed to the rest of the text and discussions. In Paper II, I formulated the research question, analysed and interpreted the mooring data, linked them to reanalysis and satellite data (atmosphere, sea ice), made the figures and wrote and submitted the paper. In Paper III, I had the principle role in designing, setting up and running the model experiments, performing the data analysis, preparing the figures, as well as writing, submitting and reviewing the paper.

Contents

Chapter 1

Motivation

Ice fronts are massive walls of ice that emerge at the floating terminus of the Antarctic Ice Sheet and extend several hundred meters deep into the ocean (Fig. 1.1). The gap between the ice front and the ocean floor is the gateway for oceanic heat to enter the vast cavities that lie beneath the ice shelves. Oceanographic observations close to the ice fronts are scarce, due to their remoteness and the extreme environment. A detailed understanding of the ocean dynamics at the ice fronts is lacking, although the ocean heat that enters the ice shelf cavities is decisive for the future of the Antarctic Ice Sheet (*Holland et al.*, 2020, *Jacobs et al.*, 1992, *Pritchard et al.*, 2012, *Rignot et al.*, 2013).

The Antarctic Ice Sheet covers 99% of the Antarctic continent and is the largest reservoir of freshwater on Earth. Its contribution to sea level rise is identified as the largest source of uncertainty for future predictions (*Joughin and Alley*, 2011, *Pattyn and Morlighem*, 2020, *Stocker et al.*, 2013). The ice sheet, up to 4.8 km thick at its maximum (*Fretwell et al.*, 2013), has formed from accumulated snow and slowly flows into the ocean under its own weight. At the so-called grounding line, the ice detaches from the ground and forms floating ice shelves that fringe three-quarters of the continent. The ice shelves mechanically support the grounded ice sheet (*Reese et al.*, 2018); thus, if they thin or disappear, the grounded ice accelerates and loses mass to the ocean, causing sea level rise (*Pritchard et al.*, 2012, *Shepherd et al.*, 2018). The West Antarctic Ice Sheet rests on a bed that deepens inland, and a retreat of the grounding line may trigger irreversible ice sheet retreat (*Joughin and Alley*, 2011, *Schoof*, 2007, *Thomas*, 1979). Since the 1990s, ice shelves in West Antarctica have thinned at an accelerating rate (*Paolo et al.*, 2015, *Rignot et al.*, 2014), mainly due to basal melting through the intrusion of warm ocean water into the ice shelf cavities (*Pritchard et al.*, 2012). The stability of the West Antarctic Ice Sheet strongly depends on the variability and future trend of the ocean heat flux, and there is a need to quantify the heat transport into the ice shelf cavities.

The ocean heat that threatens the West Antarctic Ice Sheet origins from relatively warm Circumpolar Deep Water (CDW) found north of the continental shelf (*Orsi et al.*, 1995). The CDW is located beneath a layer of cold Antarctic Surface Water (AASW) and does not reach onto the continental shelf in most regions around Antarctica (*Jenkins et al.*, 2016). In the Amundsen and Bellinghausen Sea in West Antarctica, however, CDW is found on the continental shelf.

The warm water is transported towards the ice shelves through troughs that have been incised into the seafloor by paleo-ice streams and steer the currents southward (*St-Laurent et al.*, 2013, *Thoma et al.*, 2008, *Walker et al.*, 2007). Topography strongly dictates the pathways of ocean flow, but typically only the bed topography is studied. The ice fronts are the only topographic feature in the world's ocean that intrudes the water column from above. Due to the abrupt change in water column thickness, the ice fronts pose a topographic barrier for depth-independent flow. It is of large relevance for ice shelf basal melting how the ocean currents proceed into the ice shelf cavities, but there is still a lack of knowledge on the dynamics governing the flow of warm water towards the ice shelves and into the underlying cavities.

The ice front is a particularly challenging region to study. Ship observations are restrained due to heavy sea ice during winter, the danger of calving icebergs, and instruments that fail in the cold environment (*Rintoul et al.*, 2012). Mooring arrays can typically only measure the water column below 300 m to avoid the moorings being run over by icebergs, and they only provide observations from one location. For numerical ocean models, one of the constraints is the steep topography at the continental shelf break and the ice front. The models struggle to simultaneously represent the step-topography at the front and the smoother topography on the continental shelf and at the base of the ice shelves (*Dinniman et al.*, 2016, *Kimura et al.*, 2013, *Losch*, 2008). In addition, the small Rossby radius at high latitudes demands a resolution of at least 1 km to resolve mesoscale and smaller processes that become important at the topographic barriers (*St-Laurent et al.*, 2013). Such a high resolution is computationally expensive and requires the parameterization of processes that are of particular interest in the ice shelf regions.

Ice fronts are not only impressive walls of sheer ice, but also crucial in regulating Antarctica's contribution to global sea level rise. In this thesis, I want to unveil the control of the ice fronts on the ocean heat transport that reaches the Antarctic Ice Sheet. This integral study combines observations, numerical modelling, and laboratory experiments to advance our understanding of the largely unknown ocean dynamics in the vicinity of the ice front.

Figure 1.1: The front of the Getz Ice Shelf in the Amundsen Sea, West Antarctica. Image Credit: NASA/Jeremy Harbeck[1]

[1]https://www.nasa.gov/image-feature/getting-to-know-the-getz-ice-shelf, accessed: March 21, 2021

Chapter 2

Background

2.1 The region

2.1.1 The Amundsen Sea

The Amundsen Sea continental shelf in the southern Pacific was first reached by the HMS Resolution with Captain James Cook in 1774 (*Jacobs et al.*, 2012, see the location of the Amundsen Sea in Fig. 2.1). The harsh conditions in the region did not permit them to get any further than the continental shelf break, where the deep ocean transitions to the shallow shelf seas. Until early 1994, when the US Research Vessel Icebreaker Nathan B. Palmer went to explore the Amundsen Sea coast (*Jacobs et al.*, 1996), it remained the least explored region in the Southern Ocean (*Jacobs et al.*, 2012). The area was deemed to be of little scientific interest due to the lack of bottom water formation (*Jacobs et al.*, 2012, *Orsi et al.*, 1995). However, during the expedition with RV Palmer to the Pine Island Glacier in the eastern Amundsen Sea, basal melt rates were estimated to be $10\,\mathrm{m\,yr^{-1}}$, which is an order of magnitude higher than estimates from the larger ice shelves around Antarctica (*Jenkins et al.*, 1994). These high melt rates were linked to the observed warm modified CDW with temperatures of $3\,^{\circ}\mathrm{C}$ above the freezing point close to the ice front. The relevance of the Amundsen Sea for the stability of the West Antarctic Ice Sheet started to be recognized.

Today, it is well known that the ocean temperatures on the Amundsen and Bellingshausen Sea continental shelves are higher than in most other coastal regions around Antarctica (Fig. 2.1; *Heywood et al.*, 2016, *Jenkins et al.*, 2016, *Pritchard et al.*, 2012, *Shepherd et al.*, 2018). Due to the consequences of the relatively high ocean temperatures for the ice shelves (Section 2.3), the interest in the ocean circulation has grown. A large scientific effort has helped to understand the processes that drive the oceanic heat onto the continental shelf (Section 2.2.3). The transport of the ocean heat is strongly controlled by the troughs that cross-cut the continental shelf from the shelf break towards the ice shelves (Fig. 2.2a). The highly variable surface winds, the constantly changing sea ice cover, and the buoyant meltwater from the ice shelves drive the ocean circulation and the changes in heat content.

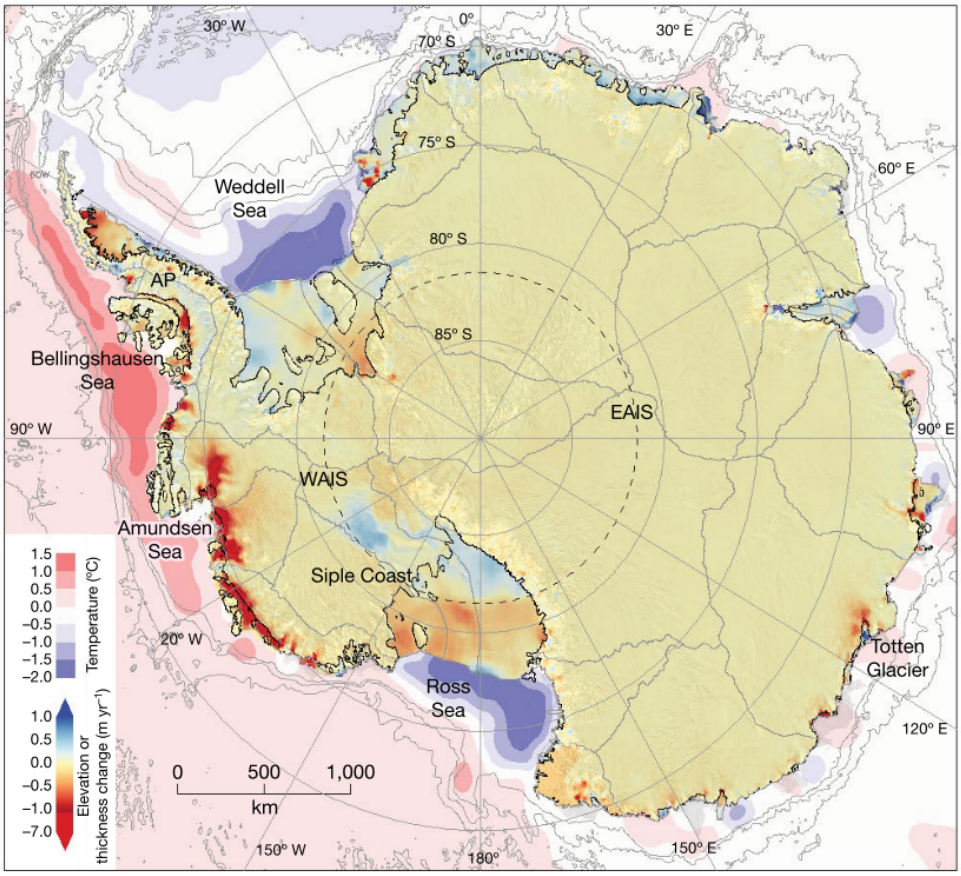

Figure 2.1: Average trend in the elevation of the Antarctic Ice Sheet and the thickness of the fringing ice shelves between 1992 and 2017. Also shown is the depth and the bottom temperature of the surrounding ocean. Thinning rates are highest in the Amundsen Sea, where warm water is found on the continental shelf. WAIS = West Antarctic Ice Sheet, EAIS = East Antarctic Ice Sheet. From Shepherd et al. (2018).

2.1.2 Atmospheric conditions

Surface winds along the coast of the Amundsen Sea are prevailing easterly and weaken northward towards the center of the Amundsen Sea Low, a climatological low pressure in the southern Pacific between 60–70°S and 60–180°W (*Turner et al.*, 2013). The shelf break in the eastern Amundsen Sea is located at roughly 72°S, where winds are generally weak or westerly. The shelf break in the western Amundsen Sea is located further south, where strong easterly winds prevail (Fig. 2.2b). Closer to the coast, katabatic winds are directed off-shore as they drain cold air down-slope the ice sheet. The Amundsen Sea experiences large variability as a result of the seasonal migration of the Amundsen Sea Low (*Raphael et al.*, 2016, *Thoma et al.*, 2008), and interannual variability can be attributed to two modes of climate variability, the El Niño-Southern Oscillation (*Paolo et al.*, 2018) and the

Southern Annual Mode (*Marshall*, 2003). Surface winds over the shelf break and on the continental shelf have direct implications for the ocean circulation (*McKee and Martinson*, 2020), the transport of CDW onto the continental shelf (*Clem et al.*, 2017, *Dotto et al.*, 2020), and the sea ice cover (*Holland and Kwok*, 2012).

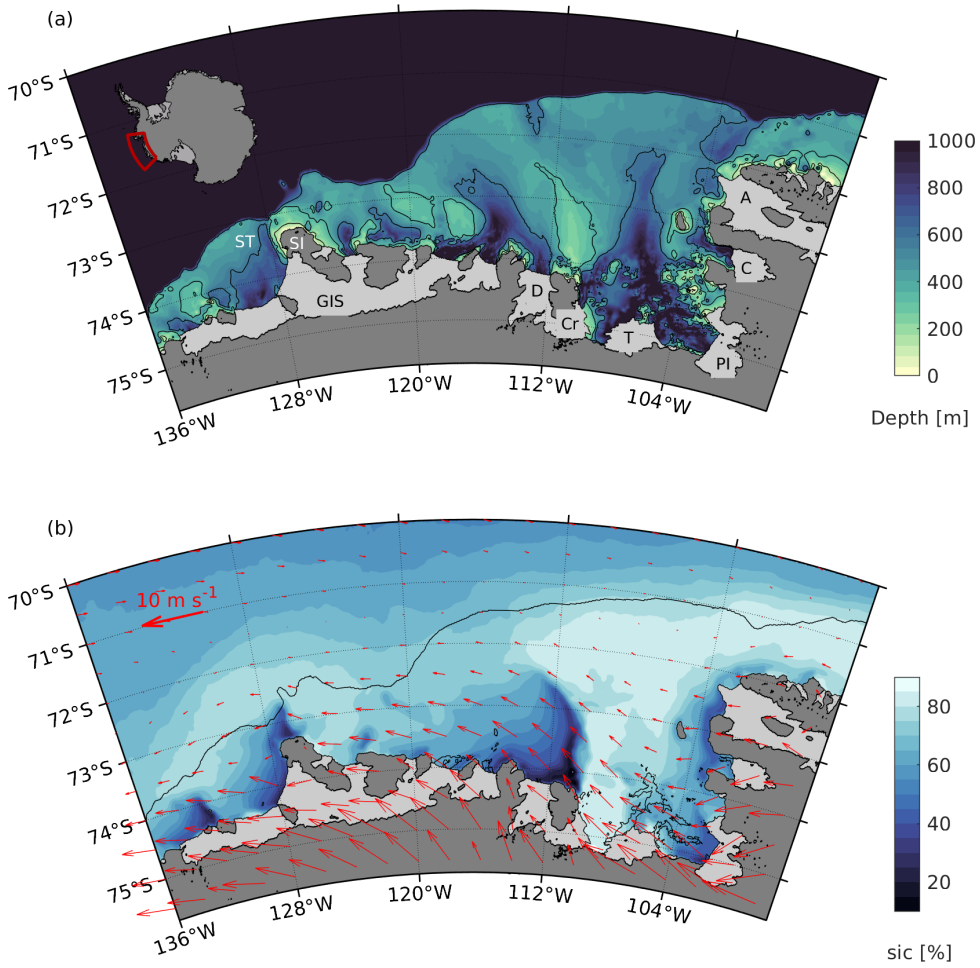

Figure 2.2: (a) Bathymetry map of the Amundsen Sea (Arndt et al., 2013). Contours show 200, 400 and 600 m depths. Ice shelves are marked in light grey land/ grounded ice in dark grey. The inset shows the location in Antarctica. The names of the ice shelves from the west to the east are: Getz (GIS), Dotson (D), Crosson (Cr), Thwaites (T), Pine Island (PI), Cosgrove (C) and Abbot (A). The Siple Trough (ST) and Siple Island (SI) are labelled. (b) Sea ice concentration from Uni Bremen (Spreen et al., 2008) (color) and 10 m-winds from ERA5 (Hersbach et al., 2018) (red arrows) averaged over the period 2012-2020 are shown.

The Amundsen Sea is covered by heavy sea ice south of 65°S during austral winter, but much of the sea ice melts during summer. In contrast to the rest of the Southern Ocean, the Amundsen Sea has experience sea ice retreat at least since 1979 (*Hobbs et al.*, 2016). The coast is characterized by the opening of several

coastal polynyas—open water within the sea ice—in regions where strong winds are directed off-coast (Fig. 2.2b). Coastal polynyas occur along the western Getz Ice Shelf, north of the Dotson Ice Shelf (the Amundsen Polynya), and along the coast north of Pine Island Ice Shelf (see Fig. 2.2b and Fig. 2.2a for location names). Coastal polynyas also form downstream of stranded icebergs and fast ice north of Crosson ice Shelf and north/east of Siple Island (*Mazur et al.*, 2017). Polynyas produce dense water, as the ocean surface is constantly cooled to the freezing point and enriched in salinity through brine release from growing sea ice that is pushed away. The variable sea ice cover modifies momentum, heat and salt fluxes at the air-ocean interface, influencing the ocean circulation and the stratification. Atmosphere-ocean interaction is consequently complex in ice-covered areas. The influence of surface processes related to winds and coastal polynyas on the heat transport into an ice shelf cavity is studied in Paper II.

2.1.3 The Getz Ice Shelf

The Getz Ice Shelf spans 650 km of the coast in the Amundsen Sea and is the largest ice shelf in the region (*Paolo et al.*, 2015). Compared to ice shelves in the eastern Amundsen Sea, the Getz Ice Shelf has a smaller drainage area (*Shepherd et al.*, 2018), and the acceleration of grounded ice due to ice shelf thinning reaches less far inland (*Reese et al.*, 2018). However, the grounding line has retreated (*Christie et al.*, 2018), the upstream grounded ice has thinned (*Pritchard et al.*, 2009, *Shepherd et al.*, 2019), and the mean ice speed has increased by 24% between 1994 and 2018 (*Selley et al.*, 2021). The Getz Ice Shelf has been one of the largest contributors to sea level rise in Antarctica (*Shepherd et al.*, 2019). Satellite estimates have shown an ice loss of 315 Gt since 1994, which corresponds to a contribution of 0.9 ± 0.6 mm to the global mean sea level rise (*Selley et al.*, 2021). The Getz Ice Shelf has also been the largest producer of meltwater in the Amundsen Sea, with ice shelf-wide basal melt rates of about $4\,\mathrm{m\,yr^{-1}}$ (*Depoorter et al.*, 2013) and up to $26\,\mathrm{m\,yr^{-1}}$ at the grounding line (*Jacobs et al.*, 2013). The meltwater may influence the ocean circulation (*Nakayama et al.*, 2014), melt rates at downstream ice shelves (*Jourdain et al.*, 2017), sea ice formation (*Jourdain et al.*, 2017) and dense water production in the Ross Sea further west (*Jacobs et al.*, 2002, *Nakayama et al.*, 2014, *Silvano et al.*, 2018).

Ocean heat from the continental shelf can enter the Getz Ice Shelf cavity at several ice fronts that are separated by islands (Fig. 2.2). The ocean temperature varies at the different entrances. While the water east of Siple Island and furthest west is rather cold, relatively warm water is found west of Siple Island (*Jacobs et al.*, 2012), where temperatures up to 1.5 °C exceed those found in front of other ice shelves in the region (*Assmann et al.*, 2019). The eastern fronts of the Getz Ice Shelf are reached by modified CDW through the Dotson-Getz trough, where a relatively persistent inflow has been observed (*Arneborg et al.*, 2012, *Wåhlin et al.*, 2013). Until the Amundsen Sea expedition with the research vessel IBRV Aaron in 2016, when the moorings in Paper I and III were deployed, observations at the western Getz Ice Shelf were limited to two cruises in 2000 and 2007 (*Jacobs et al.*, 2013).

2.2 Heat transport towards the ice shelves

Oceanic heat transport is determined by the ocean temperature and the ocean circulation. The temperature is associated with the predominant water mass that is either advected laterally by ocean currents or formed locally through heat and salt fluxes at the air-ice-ocean interfaces. Ocean currents are typically driven by buoyancy and wind forcing, inducing two distinct types of circulation modes—barotropic and baroclinic circulation—that interfere differently with topography and are of importance for the heat transport towards the ice shelves.

2.2.1 Baroclinic and barotropic circulation

Current velocities determine the rate at which water is transported. Ocean currents typically have both a barotropic and a baroclinic component that differ in their driving forces and circulation pattern. Barotropic flow is depth-independent and driven by gradients in the sea surface height. In a barotropic fluid, the density is only a function of pressure, and surfaces of constant pressure (isobars) are parallel to surfaces of constant density (isopycnals). Baroclinic flow, on the other hand, is depth-varying and driven by horizontal density gradients. In a baroclinic fluid, isopycnals are tilted relative to isobars. Figure 2.3 shows examples of a barotropic and a baroclinic, dense flow visualized in the laboratory.

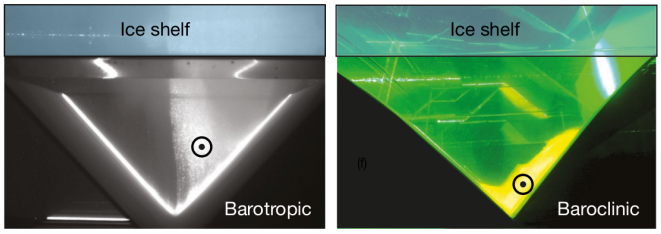

Figure 2.3: Visualization of a barotropic and a baroclinic current created in a v-shaped channel on a rotating platform. The barotropic current is set up through pumping water of the same density as the ambient water, and the baroclinic current is set up through pumping denser water into the channel. The dots with the circle symbolize the velocity out of the plane. Figure from Paper I (Wåhlin et al., 2020).

In the Southern Ocean, gradients in the sea surface height and associated barotropic flow are strongly driven by tides (*Padman et al.*, 2018) and winds (*Vivier et al.*, 2005). The Southern Ocean is the region with the strongest and most variable wind stresses in the world which points to the prominence of wind-driven, barotropic flow. The variability of winds has time scales of a few days to decades and is strongly related to the Southern Annual Mode (*Thompson and Wallace*, 2000). Variation in alongshore wind stresses close to the coast can trigger westward propagating signals, such as topographic Rossby waves (*Hughes et al.*, 2019, *Wåhlin et al.*, 2016) and barotropic Kelvin waves that can rapidly propagate along the coast (*Spence et al.*, 2017, *Webb et al.*, 2019). Tides induce high frequency (daily) variability. Around Antarctica, the tidal signal is largest in the

Weddell Sea, where strong tidal currents align with the ice front and the continental shelf break (*Padman et al.*, 2018). Although tides are generally barotropic, baroclinic tides can be induced where the topography is steep and vertical shear disturbs the stratification (*Robertson*, 2005).

Horizontal density gradients and associated baroclinic flow occur when vertical stratification is disturbed or water masses differ horizontally. Depth-varying velocities relate to density gradients through the thermal wind balance (e.g. *Cushman-Roisin and Beckers*, 2011), which states that the horizontal density gradients can be maintained due to the Coriolis force. Baroclinic flow can be generated in a stratified fluid by vertical shear induced by friction, flow across topography or wind-driven Ekman pumping. On the Southern Ocean continental shelf, a meltwater-driven baroclinic flow occurs along the base of the ice shelves, and a baroclinic depth-intensified current enhances the flow of dense CDW towards the ice shelves.

In the Amundsen Sea, the currents that transport the heat towards the ice shelves have both a barotropic and a baroclinic component. The wind-forced barotropic component explains most of the variability in the heat transport, while the baroclinic, bottom-intensified flow is persistently southward (*Arneborg et al.*, 2012, *Wåhlin et al.*, 2013). The relative importance of the barotropic and baroclinic component likely varies spatially and in time, depending on the prevalent driving mechanisms (*Kalén et al.*, 2016). While the total heat flux is the sum of the barotropic and baroclinic heat transport, the two components are expected to interfere with the ice shelf in different ways due to their unlike vertical structure.

2.2.2 Conservation of potential vorticity

In the absence of friction, barotropic flow has to conserve potential vorticity (PV) (e.g. *Cushman-Roisin and Beckers*, 2011), a concept that is of vital importance for the ocean circulation, particularly where the flow intersects with topographic features. The conservation of PV states that any changes in the water column thickness H are balanced by changes in latitude (expressed by the Coriolis parameter f) or rotation, i.e., relative vorticity $\zeta = \frac{\partial v}{\partial x} - \frac{\partial u}{\partial y}$:

$$PV = \frac{f + \zeta}{H}. \tag{2.1}$$

An important characteristics of barotropic flow that leads to this balance is that the pressure force is a conservative force and its curl vanishes. If the bottom topography changes smoothly, the flow will either shift north or south or create relative vorticity. If changes in the water column thickness are large, the flow may not be able to cross from shallow to deep (or vice versa), which is called topographic blocking (*Stewart*, 2008). As a first approximation, inertial processes can be neglected and generation of relative vorticity is considered to be small. Such a geostrophic, homogeneous flow follows lines of constant f/H. On a regional scale, where the Coriolis parameter is nearly constant, the flow aligns with lines of constant water column thickness, thus it follows the topography. Lines of constant water column thickness are equivalent to lines of constant depth (isobaths) in the open ocean, but not beneath ice shelves that intrude the water column from above.

Baroclinic flow is depth-varying, and the water column is not vertically rigid. Baroclinicity adds an additional term to the vorticity equation, because the density does not only depend on the pressure, and the curl of the pressure force is non-zero. For simplicity, a baroclinic fluid may be divided into vertically separated layers, each with its own thickness and density. Different layers of densities are separated by the pycnocline, at which the density gradient is largest. Then, conservation of PV can be applied as in Eq. 2.1 to each of the layers (e.g. *Cushman-Roisin and Beckers*, 2011). Due to the vertical separation of the density layers, topographic features do not influence the whole water column for a baroclinic fluid.

This thesis is part of the project TOBACO: "Topographic Barriers Controlling Warm Water Inflow And Antarctic Ice Shelf Melting". The two topographic barriers addressed in the project are the continental shelf break with a more regional focus on the Filchner-Trough in the Weddell Sea, and the ice front with a regional focus on the Getz Ice Shelf in the Amundsen Sea. The latter barrier is focus of this thesis. Specifically, Paper I and III build on the theory of topographic blocking and assess the influence of the ice front on a barotropic and a baroclinic current (Paper I) and the vorticity dynamics of the barotropic flow at the ice front (Paper III).

2.2.3 Flow of CDW onto the continental shelf

The water on the Antarctic continental shelves is generally cold and protects the ice shelves from the warmer water that circulates the continent with the westward Antarctic Circumpolar Current. This warm and saline CDW north of the continental shelf is located at subsurface depth (below 300 m) (*Orsi et al.*, 1995), separated from the cold and relatively fresh AASW by the Antarctic Slope Front, which marks a strong gradient in water mass properties at the continental shelf break (*Heywood et al.*, 2004, *Jacobs*, 1991). Prevailing easterly winds over the continental shelf break cause an onshore Ekman transport at the surface that deepens the Antarctic Slope Front towards the continental shelf and drives the westward Antarctic Slope Current (*Heywood et al.*, 2004, *Sverdrup*, 1953, *Thompson et al.*, 2018). The westward current is surface enhanced and decreases with depth due to the thermal wind balance, through which the tilt in density surfaces of the Antarctic Slope Front can be maintained. At depth, there is an eastward undercurrent (*Chavanne et al.*, 2010, *Walker et al.*, 2013) parallel to the continental slope.

For the CDW to flow onto the continental shelf, it has to pass both the topographic barrier posed by the continental shelf break and the dynamical barrier posed by the Antarctic Slope Front. In the Amundsen Sea, the CDW is situated less deep and reaches closer to the continental shelf than in other regions around Antarctica. The Antarctic Slope Front is less well defined, allowing an easier access onto the continental shelf, especially where troughs cross-cut the continental shelf and lower the topographic barrier at the shelf break (Fig. 2.2a; *St-Laurent et al.*, 2013, *Thoma et al.*, 2008, *Walker et al.*, 2007). Processes that control the transport of CDW onto the continental shelf in the Amundsen Sea are related to

the strength of the undercurrent (*Dotto et al.*, 2020, *Walker et al.*, 2013), bottom Ekman dynamics (*Wåhlin et al.*, 2012), eddies (*Palóczy et al.*, 2018, *Stewart et al.*, 2018, *Thompson et al.*, 2014) and surface winds (*Assmann et al.*, 2013, *Thoma et al.*, 2008, *Wåhlin et al.*, 2013, *Walker et al.*, 2013).

2.2.4 Heat transport across the ice front

The ice front is expected to be a topographic barrier to barotropic flow due to the conservation of PV. A separation of the wind-driven circulation on the continental shelf from the cavity circulation by the ice front has been shown by (*Grosfeld et al.*, 1997) with a coarse resolution model. This thesis focuses on observing the effects of the ice front with in-situ measurements and laboratory experiments, and to assess the vorticity dynamics at the ice front with a model. Here, I will outline different processes that have been found to allow cross-ice front exchange and mechanisms that drive the heat transport variability into the ice shelf cavity.

The flow in front of cold water cavities, such as the cavity of the Filchner-Ronne Ice Shelf in the Weddell Sea, has typically a strong barotropic component along the front from east to west, with only a smaller baroclinic component beneath the ice shelf draft directed into the cavity (*Foldvik et al.*, 2001). The inflow into the cavity is highly seasonal. During wintertime, the water column is nearly homogeneous due to convective mixing through sea ice growth and has a dominating barotropic component (*Nicholls et al.*, 2003). When coastal polynyas open in front of the ice shelf, eddies develop through baroclinic instabilities at the front between the dense polynya water and the adjacent water; these eddies allow an inflow into the cavity in late winter (*Årthun et al.*, 2013). In late summer, flow into the cavity results from the formation of a summertime mixed layer that sets up a strong density gradient that allows a vertical decoupling of the water column (*Nicholls et al.*, 2003). Also tides increase the exchange between the ice shelf cavity and the adjacent continental shelf (*Makinson and Nicholls*, 1999), as the steep topography induces baroclinic tides due to shear instabilities and consequently mixing (*Robertson*, 2005). Although the tidal signal is only strong in the Weddell Sea (*Padman et al.*, 2018), tides are also found to increase basal melting in the Amundsen Sea, where the tidal range is relatively small (*Jourdain et al.*, 2019, *Robertson*, 2013).

In front of the warm water cavities in West Antarctica, dense modified CDW is present below the cold AASW over most of the continental shelf and is transported by a depth-intensified baroclinic current. The thermocline that separates these two layers is approximately at the depth of the ice shelf draft; variations in its depth are decisive for the volume flux of modified CDW into the cavity and the water mass that is in contact with the ice shelf base. Different surface processes on the continental shelf modify the depth of the thermocline close to the ice shelves. Coastal polynyas deepen the thermocline due to the densification through brine release and heat extraction at the surface, a process that has been observed to influence the heat content in front of the Pine Island Ice Shelf on seasonal to interannual time scales (*Webber et al.*, 2017) with implications for the basal melt rates (*St-Laurent et al.*, 2015). Polynyas may have the opposite effect during

summer, as subducted solar heated surface water enters the ice shelf cavity and increases basal melting in the vicinity of polynyas (*Stewart et al.*, 2019). On shorter time scales, the thermocline depth varies as a result of Ekman downwelling induced by the wind stress curl (*Davis et al.*, 2018) and by along-shore winds that lead to converging Ekman transport at the coast (*Kim et al.*, 2016). Coastal Ekman pumping strengthens the coastal current that flows along the coast and the ice fronts (*Kim et al.*, 2016).

Modification of the thermocline depth through wind and sea ice processes may control the heat transport into the Getz Ice Shelf cavity west of Siple Island, given the existence of a coastal polynya. The impact of wind and sea ice on the heat transport at the ice front is investigated in Paper II.

2.3 Basal melting of ice shelves

Ice shelf melting is the main motivation to study the heat transport across the ice front. Knowledge of the processes inducing basal melting helps to interpret observations on the continental shelf in context to their importance for ice shelf melting, but also to interpret the results of idealized studies with real-world ice shelves in mind.

2.3.1 The meltwater circulation

Inside the ice shelf cavity, the ocean circulation is generally cyclonic, because of the influence of the Earth's rotation. Thus, water from the continental shelf enters the cavity in the east and exits the cavity in the west after interacting with the ice shelf. Inside the ice shelf cavity, a self-sustaining vertical circulation, the so-called "ice pump" (*Lewis and Perkin*, 1986), results from the dependency of the freezing point on pressure (the freezing point decreases by 0.76 °C per 1,000 m). This overturning circulation is driven by ice shelf melting at depth, where the in-situ freezing point is lowest, and the rise of the buoyant meltwater plume along the tilted base of the ice shelf. Melt rates induced by the ice pump are highest at the grounding zone, weakening the ice sheet where it is most vulnerable (*Hughes*, 1973).

The rising meltwater plume entrains ambient water so that the plume temperature remains above the freezing point and basal melting is sustained along the plume path (*Jenkins*, 2011). Basal melt rates are determined by the amount of heat conducted into the ice and the turbulent heat flux towards the ice shelf base (*Jenkins et al.*, 2010). Both are dependent on the freezing point, but the turbulent heat flux is in addition dependent on the ambient ocean temperature and the friction velocity. As a consequence, melt rates are a quadratic function of the ocean temperature (*Holland et al.*, 2008) and have a complex spatial pattern that resembles the velocity field at the ice-ocean boundary (*Dansereau et al.*, 2013). The pathway of the circulation inside the cavity is determined by the geometry of the ice shelf cavity (*Williams et al.*, 2001), and the buoyant meltwater plume follows the complex morphology of the ice shelf base shaped for example by channels that are carved in the ice (*Little et al.*, 2009, *Mankoff et al.*, 2012,

Millgate et al., 2013). Strong basal melting reduces the buttressing effect of the ice shelf (*Liu et al.*, 2015) and might be linked to increased iceberg calving (*Liu et al.*, 2015).

Re-freezing and deposition of marine ice at the base of ice shelves has been observed in East Antarctica (e.g. *Fricker et al.*, 2001) and beneath the Filchner-Ronne Ice Shelf (*Nicholls*, 1996), but is less expected in the Amundsen Sea. Meltwater that exits the cavities rises along the ice front due to buoyancy to the surface or spreads at intermediate depths (*Garabato et al.*, 2017, *Kimura et al.*, 2017). Observations in submarine troughs on the Amundsen Sea continental shelf show that the water that recirculates northward along the western slope of the troughs has been modified by meltwater (*Ha et al.*, 2014, *Kalén et al.*, 2016). Numerical models of the Amundsen Sea show a spread of meltwater westward towards the Ross Sea, where it may influence the deep water formation and melting of downstream ice shelves (*Jourdain et al.*, 2017, *Nakayama et al.*, 2014). Thus, basal melting is of relevance for the stability of the ice sheet and for the circulation and stratification of the adjacent ocean.

2.3.2 Different modes of ice shelf melting

Jacobs et al. (1992) identified three modes of sub-ice shelf circulation associated with the different water masses found on the continental shelf (Fig. 2.4). Although the modes are geographically separated, they do not exclusively belong to one specific region, and combinations can occur.

Mode I Cold and saline Shelf Water, formed through brine rejection from sea ice growth, flows from the the continental shelf into the ice shelf cavities. The Shelf Water is close to the surface freezing point, but induces melt at depth due to the reduced freezing point, setting up the ice pump circulation (Section 2.3.1). Re-freezing occurs when the Shelf Water - meltwater mixture (Ice Shelf Water) reaches shallower depths. This mode is most common for large ice shelves like the Filchner-Ronne Ice Shelf, Ross Ice Shelf and Amery Ice Shelf.

Mode II Relatively warm and saline CDW floods the continental shelf and fills most of the cavity with its modified version. Since the modified CDW is about 3 °C above the in-situ freezing point, strong melt occurs along the ice shelf base and freezing is absent. This mode characterizes the Amundsen and Bellingshausen Sea.

Mode III Both Shelf Water and CDW are absent on the continental shelf and melting in the outer cavity is driven by the seasonally warmed Antarctic Surface Water (AASW). Melt rates in Mode III are small, but are the main cause of melting at, e.g., the Fimbul Ice Shelf in the Eastern Weddell Sea (*Hattermann et al.*, 2012) and the Ross Ice Shelf (*Arzeno et al.*, 2014).

Since the presence of CDW on the continental shelf is decisive in the Amundsen Sea through Mode II-melting, it is crucial to understand the processes that

transport the CDW onto the continental shelf and under the ice shelf. Variations in the depth of the thermocline between the warm CDW and the cold AASW may reduce the importance of Mode II (strong) melting in favor of Mode III (weak) melting. The temperature of the water mass that is in contact with the ice shelf base is crucial for basal melting, as the melt rates depend quadratically on the ocean temperature (*Holland et al.*, 2008).

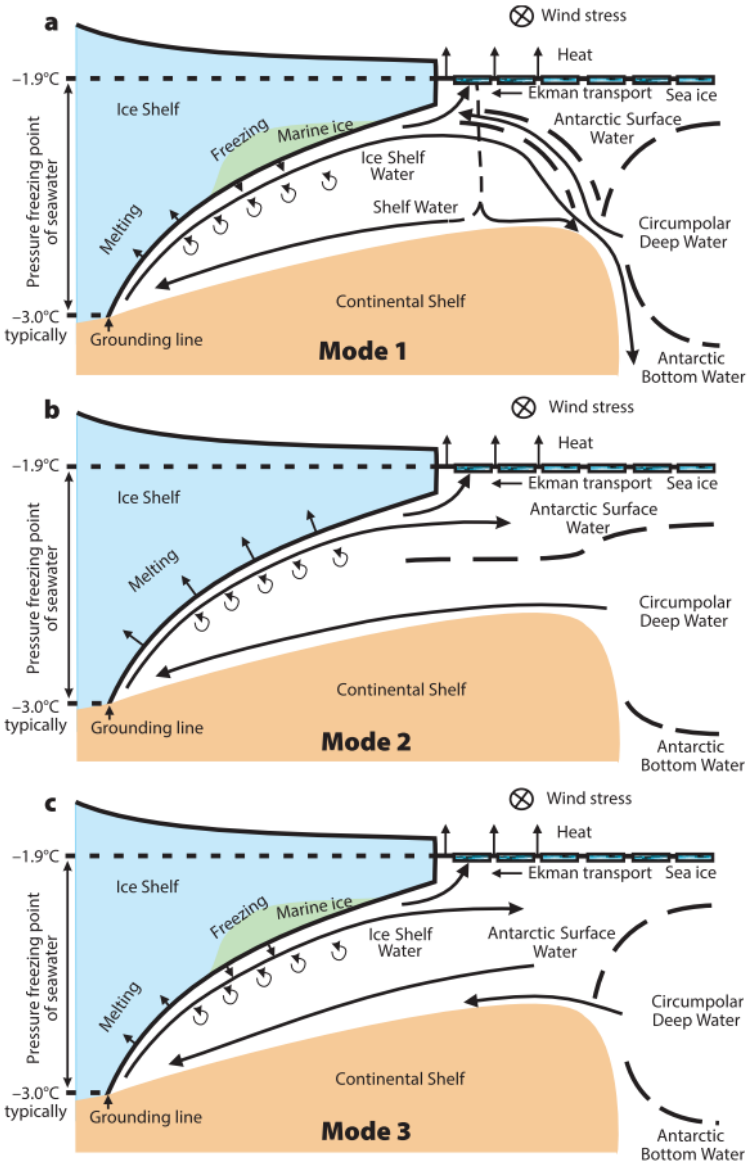

Figure 2.4: Sketch of the three different modes of ice shelf melting as first described by Jacobs et al. (1992). From Jenkins (1991).

Chapter 3

Objectives

The aim of this thesis is to provide a deeper understanding of the processes governing the flow across the ice front. The thesis is a synthesis of three scientific papers that address the following research questions based on mooring observations in front of the Getz Ice Shelf in the Amundsen Sea (Paper I+II), laboratory experiments (Paper I) and idealized numerical modelling (Paper III).

Paper I: How is the heat transport into an ice shelf cavity influenced by the ice front?

Paper II: What drives the variability of the heat transport into the Getz Ice Shelf cavity?

Paper III: How do ocean stratification and the ice shelf geometry influence the dynamics and the volume transport of a barotropic current at the ice front?

With the mooring observations, we provide an estimate of the heat transport reduction at the ice front, and we investigate the heat transport variability in response to atmospheric forcing. We use the laboratory experiments and the numerical model to assess the processes at the ice front under a controlled environment. In the laboratory experiments, we separate the barotropic and the baroclinic flow in an idealized geometry to study their individual responses to the ice front. The numerical model provides information on the dynamics at the ice front under varying conditions such as the ice front shape and background stratification.

Chapter 4

Data and Methods

The location of the oceanographic measurements (Paper I and II) at the Getz Ice Shelf is shown in Figure 4.1 together with the bathymetry that served as a model for the dimensions in the idealized numerical setup (Paper III).

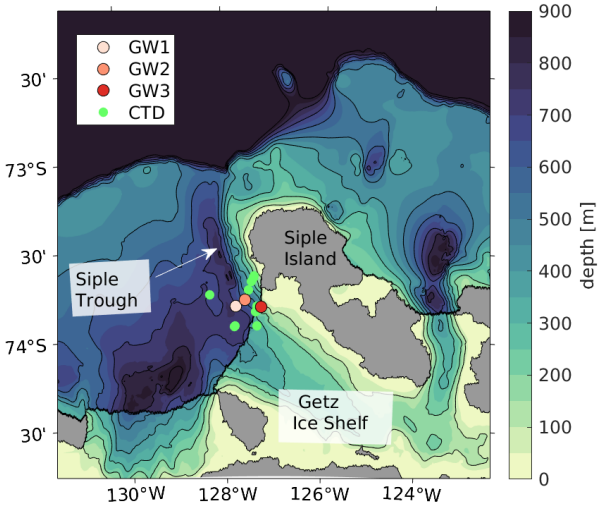

Figure 4.1: Map of the water column thickness (in color) from the RTOPO2 dataset (Schaffer et al., 2016) of the Siple Trough west of Siple Island and beneath the Getz Ice Shelf. The locations of the moorings and CTD-stations used in the papers are marked with dots. The dimensions of the trough, slope of the eastern flank and the ice shelf thickness were used as a reference for the idealized modelling.

4.1 Oceanographic data

The moorings that build the basis of the Papers I and III were deployed on January 28, 2016 during the Amundsen Sea Expedition ANA06B with IBRV Araon and recovered in January 18, 2018 during the Expedition ANA08B. Their locations,

deployment and recover data, as well as the references are given in Table 4.1. All moorings were equipped with temperature, conductivity and pressure sensors from Seabird Electronics (SBE37, SBE37, SBE56), and Acoustic Doppler Current Profilers (ADCP, Teledyne RD Instruments, 75 and 150 kHz Sentinel).

name	name in papers	longitude	latitude	depth	reference
UiB1	GW_6 (GW1)	73°S 49.800'	127°W 47.578'	707 m	*Darelius et al.* (2018)
UiB4	GW_7 (GW2)	73°S 47.671'	127°W 35.907'	601 m	*Darelius et al.* (2018)
UGOT6	GW_{6F} (GW3)	73°S 49.913'	127°W 16.546'	605 m	*Wåhlin et al.* (2019) *Wåhlin* (2019)

Table 4.1: List of the moorings used in the papers, with their original names, the names in Paper II (Paper I) and their locations, bottom depth and the references.

In addition to the mooring data, I used CTD (conductivity-temperature-density) casts obtained during the mooring deployment and recovery (*Assmann et al.*, 2019) for comparison with the linear stratification profiles used in Paper III.

4.2 Atmospheric and sea ice data

Air temperature, surface heat fluxes, 10 m winds and sea ice concentration are used in Paper III to explain the variability in thermocline depth observed at the Getz Ice Shelf. Hourly atmospheric reanalysis fields are obtained from the latest European Centre for Medium-Range Weather Forecasts (ECMWF) climate reanalysis product, ERA5, with a $0.25° \times 0.25°$ resolution (*Hersbach et al.*, 2018). The surface heat fluxes are provided as net surface latent and sensible heat, shortwave and longwave radiative fluxes.

Sea ice concentration data with a 3.125 km resolution are obtained from the University of Bremen (*Spreen et al.*, 2008). The data are based on thermal infrared (MODIS-Aqua) and passive microwave (AMSR2-GCOM_W1) satellite data. AMSR2 (Advanced Microwave Scanning Radiometer for EOS) delivers data since August 2012 and is the successor of AMSR-E on the NASA satellite Aqua, which was operation from 2002 to 2011. One example of the sea ice concentration from Uni-Bremen, ERA5 and a satellite image during a polynya opening on September 18, 2016 is given in Figure 4.2. There is a good agreement in the sea ice cover between the data from University of Bremen and the satellite image, while the ERA5 data are less detailed.

4.3 Laboratory Experiments

We conducted two sets of experiments on the Coriolis platform at the Laboratoire des Écoulements Géophysiques et Industriels (LEGI) in Grenoble. The first part focused on the flow across the continental shelf break using an idealized setup inspired by the Filchner Trough in the Weddell Sea. The second part focused on the flow into an ice shelf cavity using a setup representative of a v-shaped

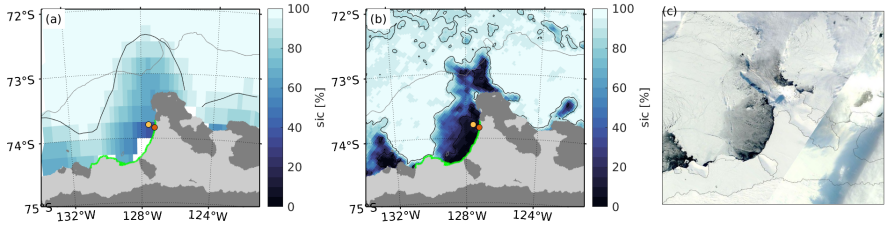

Figure 4.2: Sea ice concentration during a polynya opening on September 18, 2016 close to the mooring site. (a) Data from ERA5, (b) Data from Uni-Bremen, (c) Satellite image from MODIS. The black contour in (a) and (b) is the 90% sic. The Getz Ice Shelf is marked in light grey and land/ grounded ice is in dark grey in (a) and (b). The locations of the two moorings GW_6 and GW_{6F} used in Paper III are marked as yellow and orange dots.

channel such as the Siple Trough (Fig. 4.1). Paper I incorporates the second set of experiments. In this section, I will provide further details on the experiments, the data processing and the error estimation.

Experimental setup

The geometry of the v-shaped channel and the ice shelf used for the ice front experiments is shown in Figure 4.3 and described in detail in Paper I.

The parameters that are varied during the ice front experiments are presented in Table 4.2. The rotation speed and the flow rate determine the Rossby number and the Ekman number. The draft and tilt of the ice shelf aim to modify the blocking and the circulation inside the cavity. The density difference determines whether the generated flow is barotropic or baroclinic. Only a subset of the conducted experiments is presented in Paper I. These are highlighted in bold in Table 4.2.

Notation	Parameter	unit	values
Ω	rotation frequency	s^{-1}	**1/30**, 1/50
D	ice shelf draft	cm	**0**, 5, 10, **15**, 20, **30**, **0-30**, 0-15
Q	flow rate	l min^{-1}	15, 30, 50, **60**
$\Delta\rho$	density difference	kg m^{-3}	**0**, 1, **2**
Ro	Rossby number $(\frac{U}{fL})$	-	0.05-0.2
Ek	Ekman number (δ_E^2/H^2)	-	$2 \cdot 10^{-5}$, $\mathbf{0.9 \cdot 10^{-5}}$

Table 4.2: Parameters that are varied during the ice front experiments conducted on the rotating platform. For the cases with an ice shelf draft of 0-30 and 0-15, the draft is sloping down from 0 at the front to 30(15) in the back. For the non-dimensional numbers (Rossby and Ekman number), the velocity U varies between the experiments, the length and depth scales are $L = H = 0.5\,\mathrm{m}$ and the Ekman depth is $\delta_E = \sqrt{\nu/f}$, with $\nu = 10^{-6} m^2 s^{-1}$. Parameter values used in Paper I are highlighted in bold.

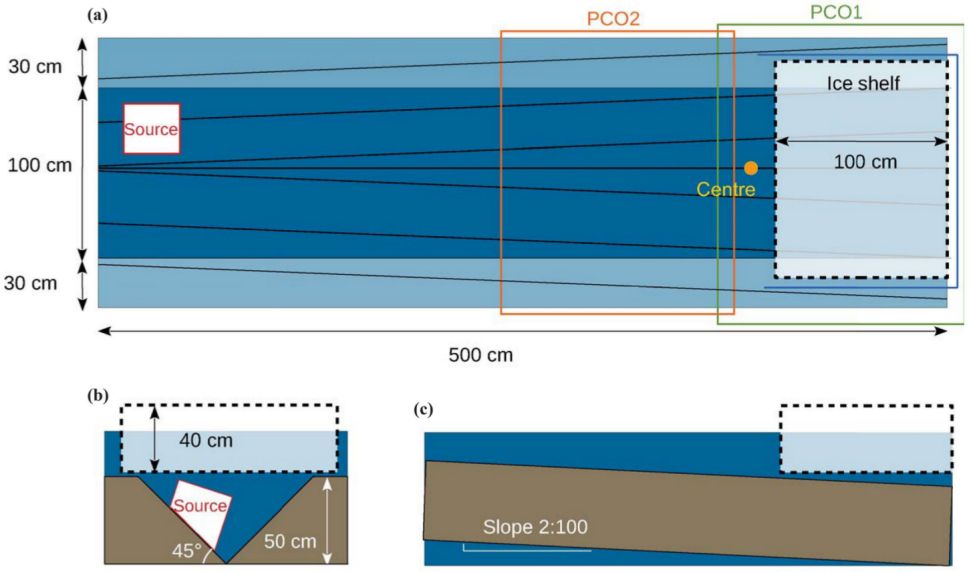

Figure 4.3: Idealized geometry of the v-shaped channel and the overlying cuboid plastic ice shelf used as a setup for the laboratory experiments on the rotating platform. (a) Top-view of the channel (dark blue) with the horizontal flanks (light blue) and the overlying ice shelf (transparent box). The location of the source and the center point of the platform are marked, as well as the view-range of the two cameras PCO1 and PCO2. (b) Cross-section of the setup looking towards the ice shelf (transparent box), with the source on the left flank of the v-shaped channel (brown). (c) Side-view of the sloping channel (brown) and the ice shelf (transparent box). Figure from Wåhlin et al. (2020).

PIV method

Two cameras above the rotating platform took pictures of the flow, where one camera focused on the channel (PCO1 with a 35 mm objective lens) and the other camera on the cavity circulation beneath the transparent ice shelf (PCO2 with 20 mm objective lens) (Fig 4.3a). The flow was seeded with neutrally buoyant micro-particles and illuminated with a laser sheet that aligned with the sloping channel (Fig. 4.3c). The channel and the ice shelf were build with transparent Plexiglas to allow the laser light to penetrate through.

We obtained velocity fields at different depths with a scanning PIV method, sketched in Fig. 4.4. The laser sheet is moved vertically by a computer-controlled carriage and stops at several depth levels $k = 1, ..., L$ to obtain a volume scan. At each depth level, the cameras take N consecutive images within one burst, before the laser sheet moves to the next level. The volume scans ($j = 1, ..., S$) are repeated continuously throughout the experiment.

Data processing

To turn the images into velocity fields, we applied Particle Image Velocimetry (PIV) using the UVMAT-software (http://servforge.legi.grenoble-inp.fr/projects/soft-

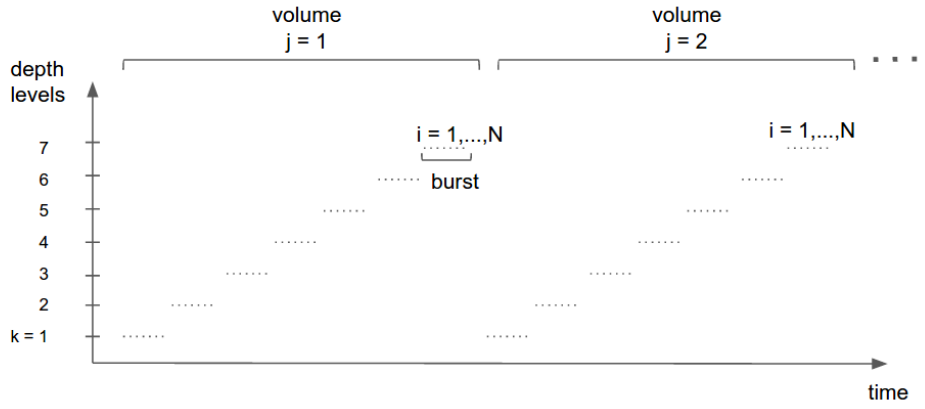

Figure 4.4: Sketch of the scanning PIV method. The dots symbolize images taken at the corresponding time step and depth level.

uvmat). Several processing steps have to be carried out to obtain the final velocity field. The different steps are illustrated in Fig. 4.5 using one of the experiments. First, the original images (Fig. 4.5a) are transformed to physical coordinates relative to a reference zero-point at the ice front. The transformation parameters are determined from images of a horizontal and an inclined grid taken with the same camera and laser setup as used in the experiments. Then, the topography is masked and the brightness of the stationary background is removed (Fig. 4.5b). Each image is subdivided into small correlation boxes, large enough to contain at least 5 particles (here: size = 33 × 33 px) (Fig. 4.3c). From one image to the next one, the particles within a correlation box A have moved further within a larger search box (here: size = 65 × 65 px). The displacement ($\boldsymbol{dx}$) of the particle pattern within box A is obtained by maximizing the cross-correlation between the particle patterns within box A and a displaced correlation box B. For a good result, the time step between consecutive images should be large enough to have a displacement of about 5-20 px (here: $dt = 0.5\,\mathrm{s}$ for the barotropic and $0.1\,\mathrm{s}$ for the baroclinic flow). The velocity is then calculated from the displacement and the time step between the images. The resulting velocity data point is located half-way between the correlation boxes and is therefore on an irregular grid. Afterwards, the velocity data are interpolated on a regular grid with a thin shelf spline interpolation. We removed data points whenever the optimum displacement is too close (< 2px) to the boundaries of the search box and when the correlation is less than 0.1. The PIV process is repeated in a second iteration to improve the velocity field and to fill gaps.

Challenges in conducting laboratory experiments

Experiments are deemed to go wrong and we encountered a number of challenges and issues during the conduction of the experiments, which I m briefly discussing here.

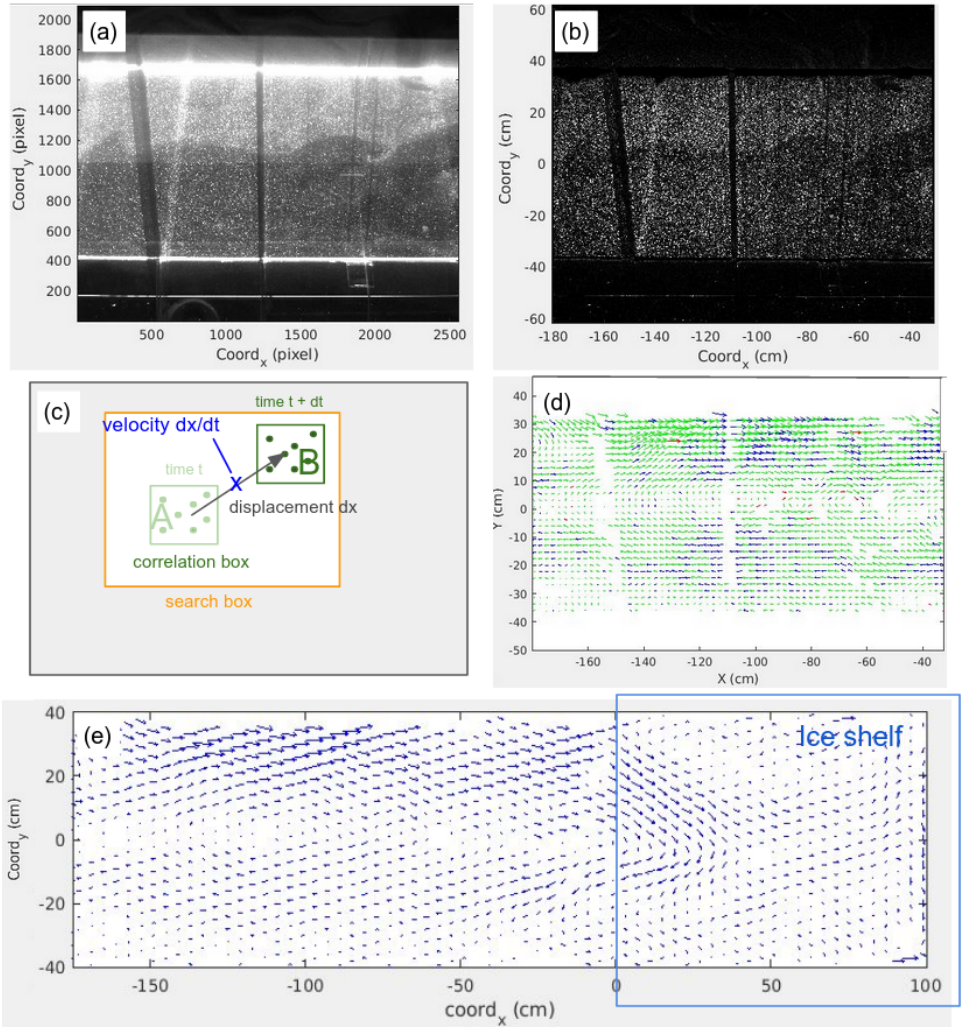

Figure 4.5: Different steps of the particle image velocimetry (PIV). (a) Raw image of the flow taken with the camera PCO2 over the channel. (b) The background brightness is removed from image (a) and the coordinate system transformed into cm relative to a fixed point. (c) Sketch of the correlation processes to calculated the velocity. (d) Final velocity field of PCO2 with bad data removed. (e) The combined velocity field of PCO1 and PCO2 with only every 4th vector shown after two iterations of PIV and applying a thin shelf spline interpolation.

- Controlling the water density: For the barotropic flow, the density in the source water had to be equal to the density of the tank water. Although the temperature in the room was strictly controlled, the source water was stored in a smaller tank above the platform and tended to be slightly warmer. We balanced differences in temperature by adding salt to the source tank.

- Solid body rotation: It takes about two to three hours for the water to return to steady-state after an experiment, but the remaining background

movement of the particles was sometimes recognized after processing the data. The background movement was typically negligible compared to the velocity of the injected flow, but some experiments had to be repeated.

- Constant water level: Through the injection of the source water, the water level increased and had to be controlled continuously. We used a skimmer to drain excess water and we manually measured the water depth frequently.
- Surface waves: Small disturbances of the water surface created surface waves visible in the images. This problem was enhanced by the ice shelf sitting at the water surface, as it was attached to the small platform that we worked on.
- Unsteady flow: The source contained a honey-comb constructed of small pipes to create a steady, laminar flow. However, turbulence, eddies and air bubbles from the water injection created disturbances.
- Particle density: The image quality is reduced if the particle density is too low or too high. We had to steer up the particles from the floor frequently and add the right amount of particles to the source water.

I consider the communication of the encountered challenges and experiences as an important part of the laboratory work, as fellow scientists can learn from them and be prepared.

4.4 Idealized Modeling

In Paper II, I use the Massachusetts Institute of Technology general circulation model (MITgcm) (*Adcroft et al.*, 2018, *Marshall et al.*, 1997a,b) to set up an idealized numerical model of a submarine trough and an ice shelf (*Losch*, 2008), inspired by the laboratory experiments in Paper I. The advantage of the numerical modeling over laboratory experiments is to better resolve the ice front region, where the laboratory data are of poor quality, and to include and control further parameters such as stratification and basal melt. In the numerical model setup, I increased the dimensions to match a real-size ice shelf system. I added a flat region in the center of the trough, which compares better to real sub-marine troughs and is dynamically interesting, as the circulation inside and outside the ice shelf cavity is expected to be separated over flat bathymetry (*Grosfeld et al.*, 1997). In the numerical model, thermodynamic interactions between the ice shelf base and the ocean can be turned off. In that case, there is no basal melting and no circulation related to the “ice pump”, such that a purely barotropic current can be studied. However, the thermodynamic interaction is turned on in some of the experiments to investigate the impact of the cavity circulation induced by the externally forced barotropic current on the basal melt rates. Details on the model setup and the conducted experiments are provided in Paper II.

Chapter 5

Summary of the results

Paper I: Ice front blocking of ocean heat transport to an Antarctic ice shelf

Wåhlin, A.K., Steiger, N., Darelius, E., Assmann, K.M., Glessmer, M.S., Ha, H.K., Herraiz-Borreguero, L., Heuzé, C., Jenkins, A., Kim, T.W., Mazur, A.K., Sommeria, J., Viboud, S. (2020), Nature, 578

Paper I combines mooring observations, laboratory experiments and theory to investigate the influence of an ice front on the heat transport into ice shelf cavities. Three moorings in front of the Getz Ice Shelf in West Antarctica measured ocean currents and temperature from January 2016 to January 2018. Two moorings at 11 and 14 km distance from the ice front show that the ocean heat was transported towards the ice shelf along the eastern slope of the Siple Trough, by a southward current that has a dominating barotropic (depth-independent) component compared to the smaller baroclinic (depth-intensified) component. Only about one sixth of the southward heat transport reached the third mooring at 800 m distance to the ice front. This remaining heat transport is associated with the baroclinic component of the along-trough current. The barotropic component of the current is blocked by the ice front, unable to enter the ice shelf cavity.
We reproduced the behaviour of the current at the ice front on a rotating table, where barotropic and baroclinic currents were generated by pumping fresh and dense (saline) water, respectively, into an idealized v-shaped channel overlaid by a cuboid Plexiglas ice shelf. In the barotropic experiments, the ice front deflected the current to the right. In the baroclinic experiments, the dense current entered the ice shelf cavity freely. In agreement with geostrophic theory and the vertical rigidity of barotropic flow, the barotropic current follows lines of constant water column thickness, while the baroclinic dense current follows lines of constant bathymetry. This explains the observed blocking of the barotropic current at the front of the Getz Ice Shelf.

Paper II: Intermittent reduction in ocean heat transport into the Getz Ice Shelf cavity during strong wind events

Steiger, N., Darelius, E., Wåhlin, A. and Assmann, K., submitted to GRL

Paper II investigates the atmospheric influence on the variability of the heat transport towards the Getz Ice Shelf. The mooring observations used in Paper I show events of intermittent thermocline deepening towards the bottom that reduce the transport of warm water towards the ice shelf cavity. The events have a time scale of a few days and coincide with strong easterly winds and the opening of a coastal polynya over the mooring site. The intermittent thermocline deepening is not directly linked to the polynya, but caused by wind-driven Ekman convergence and downwelling at the northern Siple coast, about 100 km away from the moorings. The signal propagates towards the Getz ice front along the western Siple coast via a coastal trapped wave. The near-front mooring shows that the thermocline deepening is accompanied by acceleration and an alignment of the current with the ice front during the thermocline deepening. The heat transport towards the ice shelf cavity during April to November 2016 was reduced by about 25% due to nine strong events of thermocline deepening. Almost no events occurred the following year and we suggest that interannual variability is linked to the number of strong wind events and the pre-conditioning of the water column by seasonal deepening of the thermocline through sea ice growth.

Paper III: **The dynamics of a barotropic current at an ice front**

Steiger, N., Darelius, E., Kimura, S., Patmore, R., Wåhlin, A., in review in JPO

Paper III addresses the dynamics of a barotropic current colliding with an ice front, as a direct follow up on Paper I. We use an idealized numerical model to investigate the vorticity dynamics at the ice front and the sensitivity of the barotropic induced transport into an ice shelf cavity to ice shelf thickness and stratification. In a homogeneous ocean, the externally forced barotropic flow largely follows f/H contours, apart from the ice front region where lines of constant water column thickness are discontinuous. The barotropic volume transport into the cavity consequently depends on the depth of the ice shelf base. As parts of the barotropic flow pass the ice front region, the water column gets squeezed and strong vertical velocities occur at the ice front. Relative vorticity and friction play an important role locally at the ice front for the barotropic flow to enter the cavity. The part of the barotropic flow that is blocked at the ice front develops a strong lateral current that undercuts the ice front, leading to high melt rates at the front. Parts of the barotropic flow can only enter the cavity if the ocean is weakly stratified; for stronger stratification, vertical velocities are suppressed and the externally forced barotropic flow is unable to squeeze into the cavity. Most of the barotropic flow is blocked and a broad lateral current develops along the ice front.

Chapter 6

Perspectives

6.1 Concluding remarks

The Amundsen Sea is a key region for future projections of global sea level rise. The ocean circulation in this region and the ocean heat delivery to the ice shelves have gained increasing attention during the last decades. While many studies have focused on the heat transport across the continental shelf break, the three papers presented in this thesis show that the ice front is a critical dynamic barrier that limits the heat transport that eventually enters the sub-ice shelf cavities.

The results emphasize the relevance of the vertical density and velocity structure of the water column for the heat transport into the cavity. In Figure 6.1, I summarize the influence of the ice front on an externally forced barotropic current for three stratification profiles discussed in the papers:

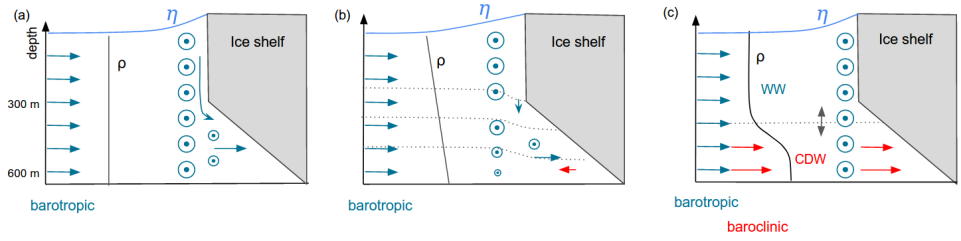

Figure 6.1: Sketch of the flow at an ice front for different stratification and inflow: (a) barotropic flow and no stratification, (b) barotropic flow and linear stratification, (c) barotropic and baroclinic flow with a pycnocline beneath the depth of the ice shelf draft. Arrows show the horizontal velocities towards the ice shelf and vertical velocities at the ice front, and circles with dots show the velocities parallel to the ice front out of the plane; blue is the barotropic and red the baroclinic component. The black vertical profile is the density-profile (ρ). Dotted lines mark the depth of the (b) isopycnals and (c) pycnocline. The black double arrow in (c) symbolizes the variability of the pycnocline depth. η is the anomaly of the sea surface height.

- *No/ weak stratification (Fig.6.1a):* Part of the externally forced barotropic flow can enter the ice shelf cavity, strongly dictated by the change in water column thickness (Paper III). High vertical velocities occur at the ice front

when the flow squeezes into the ice shelf cavity. The blocked part of the flow creates a strong boundary current that undercuts the ice front and increases basal melt rates in the frontal zone. Situations with a weak stratification occur, for example, when the surface mixed layer is pushed towards the bottom by along-shore surface winds (Paper II).

- *Linear stratification (Fig.6.1b):* When the stratification is strong enough, an externally forced barotropic component is almost entirely blocked at the ice front, as the stratification suppresses vertical velocities (Paper III). The stratification in combination with vertical shear at the ice front causes a deepening of the isopycnals towards the ice front, associated with a weak baroclinic circulation opposing the barotropic circulation at depth.

- *Strong pycnocline (Fig.6.1c):* If the barotropic flow is intensified by a baroclinic flow beneath the deep (below the ice draft) pycnocline, the two components separate at the ice front (Paper I). Only the baroclinic component enters the cavity, while the barotropic component is deflected. A deepening of the pycnocline due to coastal Ekman downwelling reduces the baroclinic heat transport into the ice shelf cavity (Paper II).

The ice shelf thickness and bottom topography dictate the extent of the topographic barrier, and the heat transport associated with the baroclinic component is decisive for the heat delivery to the ice shelf cavities. The variability of the inflow is influenced by atmospheric processes associated with winds and sea ice, as they modulate the stratification and the relative importance of the barotropic and baroclinic component. Knowledge on the baroclinic heat transport along the slopes of the channels on the continental shelf, e.g., measured by moorings, allows an estimate of the heat transport that eventually reaches into the cavities.

6.2 Open questions and future suggestions

This thesis is a complementary work based of different methods that collectively provide a better understanding of the ocean dynamics at an ice front and the controls on the heat transport into an ice shelf cavity. As every new finding, the presented studies pose more new questions than they provide answers. Here, I will present further ideas that evolved during this study with suggestions for future work.

Ice front blocking Ice front blocking of the barotropic flow is an inevitable consequence of geostrophy, and it has previously been observed at the Filchner-Ronne Ice shelf (*Foldvik et al.*, 2001) and has been studied with a numerical model (*Grosfeld et al.*, 1997). In Paper I, we revisited the effect of ice front blocking in a region, where the slope of a trough intersects the ice front and both a barotropic and a baroclinic component control the heat transport. I believe that the separation of the barotropic and the baroclinic components at the ice front and the direct consequences for the heat transport into the cavity have not been shown in such an integral way before. The consequences of the ice blocking on the Getz Ice Shelf

appear to be large, and a next step would be a compilation of the relative contribution of the barotropic and the baroclinic component to the total heat transport in other troughs; this could provide an estimate of the southward heat transport that is associated with the baroclinic component. An estimate of the transport capacity of a dense current in a downward sloping channel can also be done based on the channel shape and the thickness of the Ekman layer (*Wåhlin*, 2002, 2004). The estimated transport together with the temperature of the dense layer provides an upper estimate of the baroclinic heat transport that reaches the ice shelf cavities.

The impact of local atmospheric forcing on the heat transport The coastal waters at the margins of the ice sheet are prone to modification at the air-ocean interface due to the divergence of surface wind stress and sea ice. Surface processes related to coastal polynyas and coastal Ekman pumping control the heat content and the thermocline depth on various time scales (Paper II; *Davis et al.*, 2018, *St-Laurent et al.*, 2015, *Webber et al.*, 2017). We showed in Paper II that changes in the thermocline depth alter the volume of CDW, and possibly the relative contribution of the baroclinic component to the total heat transport, even in short distance from the ice front. Thus, it is of great interest to conduct long-term measurements close to the ice front—ideally within the Rossby radius—, in order to resolve the variability in the thermocline depth and the heat transport on different time scales. Single CTD-casts might be logistically preferred, but they are usually biased towards summer months and have to be regarded with care due to the strong variability in time. The mooring time series presented in Paper I and II provide a great insight into the variability of the thermocline depth at a distance to the ice shelf that is usually inaccessible. A prolongation of the measurements together with atmospheric data would complement the study well to provide a better understanding of the relevance of the events of thermocline deepening in a longer time frame, as well as an insight on the influence of the coastal polynya on heat transport. The strong coupling of the ocean heat transport to atmospheric conditions suggests the use of a regional sea ice-ocean coupled model to investigate the relevance of winds and sea ice growth on the variability of basal melt rates. Such a study has been presented by *St-Laurent et al.* (2015) with a focus on polynyas in front of the Pine Island Ice Shelf. It would be of interest to disentangle the relevance of wind-driven downwelling versus convection in coastal polynyas for basal melting of different ice shelves.

Investigating the impact of heat transport variability on basal melting Variability in the thermocline depth has been found to directly impact basal melt rates at several ice shelves (*Davis et al.*, 2018, *Padman et al.*, 2012, *St-Laurent et al.*, 2015), but it is unclear whether the coupling between basal melting and atmosphere-ocean conditions is representative of other ice shelves and of different time periods. The question arises whether the intermittent reduction in the heat transport in front of the Getz Ice Shelf influences the melt rates of the upstream ice shelf and whether the heat transport into the cavity estimated in Paper I is representative for the heat used to melt the ice. The melt rates and the impact of the thermocline

variability on basal melt rates can, for example, be observed with Autonomous Phase-Sensitive Radio Echo-Sounders (ApRES) placed on the ice shelf (*Davis et al.*, 2018). Four ApRES were installed on the Getz Ice Shelf downstream of the moorings during the deployment cruise to complement the ocean measurements. The instruments were unfortunately not collected (due to technical problems with the helicopters on the recovery cruise) and only a subset of the data, transferred via satellite, is available. The existing data show a tidal signal and no obvious correlation with the ocean heat content at the moorings (*Karam*, 2019). It is unclear whether there is indeed no direct impact of the variability in the heat content on melt rates or whether the impact is not visible in the data due to the location of the ApRES, poor data quality or the short time frame available. Evaluating the relevance of the daily to weekly variability in the heat transport for the ice shelf (Paper II) would benefit greatly from the collection of these instruments or the installation of new ApRES as a supplement to longer mooring time series at the ice front.

Coastal Ekman downwelling and wave propagation The process of coastal Ekman downwelling is well known, and we suggest in Paper II that downwelling at an ice front might disrupt the inflow of warm CDW into the ice shelf cavity. The downwelling can both be forced locally (*Kim et al.*, 2016) or remotely (Paper II) and may influence downstream ice shelves through a coastal trapped wave that propagates westward along the coast and through strengthening of the westward coastal current (*Kim et al.*, 2016). To confirm the presence of coastal trapped waves, several moorings would be needed along the ice front at a distance of less than the Rossby radius from the front. How often do coastal trapped waves occur and how do they influence the ice shelves? The occurrence of coastal trapped waves along the Siple Coast and the modification in heat transport at the ice front could be studied further in a regional or idealized numerical model.

In relation to Paper II, I explored the daily regional model output of the Amundsen Sea for 2016-2017 from *Nakayama et al.* (2018), which indeed shows a wind-driven wave propagation along the coast of Siple Island. The wave is visible in the 0-isotherm depth and travels from north of Siple Island towards the mooring site and along the ice front. The modelled deepening of the isotherm at the mooring site coincides with the events seen in the mooring data. Although the stratification is exaggerated in the model, leading to different wave speeds and a smaller magnitude in thermocline deepening, the model can still be used to evaluate the isotherm variability and its relevance for other ice shelves.

Another alternative is to study the processes of wind-driven coastal Ekman deepening and coastal trapped waves in an idealized polynya model. The geometry could include a coast next to a vertical ice front, and an idealized wind forcing with events of strong along-shore winds. This would allow an investigation of the magnitude and length of wind forcing needed to deepen the thermocline towards the bottom as well as the necessary preconditioning of the water column by convection in the coastal polynya.

Challenges for modelling studies In section 6.1, I conclude that the ocean heat transport into ice shelf cavities is largely controlled by the pycnocline depth, the stratification profile and the relative contribution of the baroclinic and the barotropic components. Thus, regional models that aim to estimate ice shelf melt rates need to adequately capture the stratification on the continental shelf and its variability through atmospheric forcing. Even though the heat content on the continental shelf might agree well with observation, the processes in the vicinity of the ice front are determining for the inflow into the ice shelf cavity. The largest challenges for ocean modelling in the coastal regions around Antarctica include the steep topography at the continental shelf and at the ice front, the lack of resolution in order to resolve processes at the ice front and inside the sub-ice shelf cavities and poorly known boundary conditions and atmospheric forcing. It is therefore a useful exercise to complement large-scale and regional-scale modelling with process- and idealized modelling studies similar to those presented in Paper III that allow the use of a high resolution and the investigation of individual processes that are otherwise unresolved. Another challenge is that both the bathymetry and the—constantly changing—ice shelf geometry need to be well resolved, since they strongly determine the volume transport and the pathways of the heat transport into and inside the ice shelf cavities.

Future changes In the future of the Amundsen Sea, we might expect ice shelves to thin (*Shepherd et al.*, 2018), grounding lines to retreat (*Konrad et al.*, 2018), meltwater discharge to increase (*Bronselaer et al.*, 2018) and sea ice to decline (*Parkinson*, 2019). Winds might strengthen and shift southwards as a response to a strengthening Southern Annual Mode (*Marshall*, 2003) and due to a deepening and seasonal poleward migration of the Amundsen Sea Low (*Gao et al.*, 2021). Changes in sea ice concentration and surface winds have implications for the ocean through changes in surface stresses, thus Ekman dynamics, wind-forced currents and changes in the stratification. The response of basal melting on changes in winds is complex (*Dinniman et al.*, 2012, *Donat-Magnin et al.*, 2017, *Dotto et al.*, 2019, *Spence et al.*, 2014, 2017), as it varies geographically, depends on sea ice, and can trigger changes in ocean heat transport at remote locations. Surface winds can change the strength of barotropic flow, while the wind stress curl influences the steepness of isopycnals and, thus, baroclinic flow. Sensitivity studies are well suited to tackle the impact of changing winds and sea ice concentration on the ocean circulation.

We have identified the ice shelf draft as a controlling factor for the ocean heat transport into an ice shelf cavity in Paper I + III. Firstly, the ice shelf draft relative to the thermocline depth determines whether the baroclinic component can enter the cavity freely. Secondly, the ice shelf draft relative to the depth of the sloping sea floor determines the fraction of the barotropic component that continue inside the ice shelf cavity. The baroclinic flow is expected to reach deeper towards the grounding line, while the barotropic flow might rather impact the frontal region of the ice shelf. What is the effect of ice shelf thinning on basal melt rates? Model simulations with modified ice shelf thickness of the Filchner-Ronne Ice Shelf showed a decreased tidal speed at the frontal zone for a thinner ice shelf (*Padman et al.*, 2018), which is in agreement with Paper III. However,

the volume flux into the cavity increases for a thinner ice shelf, but the ice shelf base might me in contact with typically colder waters higher up in the water column, at least for warm ice shelves. It would be interesting to investigate the impact of changing ice shelf draft with regional model simulation similar to those presented in *Padman et al.* (2018) for different regions, adding an offset to the ice shelf thickness.

Another immediate consequence of basal melting and ice shelf thinning is the retreat of the grounding lines, which is expected to increase basal melting (*Donat-Magnin et al.*, 2017) and impact the stability of the ice sheet (*Schoof*, 2007). In this thesis, I have not investigated the impact of grounding line retreat, but I believe that it adds a critical uncertainty for future predictions of the Antarctic Ice Sheet. Ocean-driven basal melting is an important factor of the ice sheet mass budget, and we need to understand the response of the ice sheet to the changes at the margins. There is a strong need to understand, when tipping points are reached that are associated with an irreversible retreat of the grounding line due to a reversed bed slope (*Pattyn and Morlighem*, 2020). To adequately simulate the future evolution, ice sheet models need a good representation of the bed topography, but also the right boundary conditions at the marine margin, or better, a coupling to the adjacent ocean. Model intercomparison projects (MIP) that explore the model skills of Marine Ice Sheet models (MISMIP), coupled Ice Shelf-Ocean models (ISOMIP) and coupled ice sheetocean experiments (MISOMIP) are a great community effort to evaluate and verify coupled models and to conduct future projections (*Asay-Davis et al.*, 2016). I believe that these model intercomparisons are an important step forward to a better understanding on the impact of ocean conditions on basal melting and the response of the ice sheet.

Bibliography

Adcroft, A. J., J.-M. Campin, E. Doddridge, S. Dutkiewicz, C. Evangelinos, D. Ferreira, M. Follows, G. Forget, B. Fox-Kemper, P. Heimback, C. Hill, E. Hill, H. Hill, O. Jahn, J. Klymak, M. Losch, J. Marshall, G. Maze, M. Mazloff, D. Menemenlis, A. Molod, and J. Scott (2018), MITgcm Documentation. 4.4

Arndt, J. E., H. W. Schenke, M. Jakobsson, F. O. Nitsche, G. Buys, B. Goleby, M. Rebesco, F. Bohoyo, J. Hong, J. Black, R. Greku, G. Udintsev, F. Barrios, W. Reynoso-Peralta, M. Taisei, and R. Wigley (2013), The international bathymetric chart of the Southern Ocean (IBCSO) version 1.0-A new bathymetric compilation covering circum-Antarctic waters, *Geophysical Research Letters*, *40*(12), 3111–3117, doi:10.1002/grl.50413. 2.2

Arneborg, L., A. K. Wåhlin, G. Björk, B. Liljebladh, and A. H. Orsi (2012), Persistent inflow of warm water onto the central Amundsen shelf, *Nature Geoscience*, *5*(12), 876–880, doi:10.1038/ngeo1644. 2.1.3, 2.2.1

Årthun, M., P. Holland, and K. Nicholls (2013), Eddy-Driven Exchange between the Open Ocean and a SubIce Shelf Cavity, *Journal of Physical Oceanography*, *43*, 2372–2387, doi:10.1175/JPO-D-13-0137.1. 2.2.4

Arzeno, I. B., R. C. Bearsley, R. Limeburner, B. Owens, L. Padman, S. R. Springer, C. L. Stewart, and M. J. M. Williams (2014), Ocean variability contributing to basal melt rate near the ice front of Ross Ice Shelf, Antarctica, *Journal of Geophysical Research: Oceans*, *119*, 4214–4233, doi: 10.1002/2014JC009792. 2.3.2

Asay-Davis, X. S., S. L. Cornford, G. Durand, B. K. Galton-Fenzi, R. M. Gladstone, G. Hilmar Gudmundsson, T. Hattermann, D. M. Holland, D. Holland, P. R. Holland, D. F. Martin, P. Mathiot, F. Pattyn, and H. Seroussi (2016), Experimental design for three interrelated marine ice sheet and ocean model intercomparison projects: MISMIP v. 3 (MISMIP +), ISOMIP v. 2 (ISOMIP +) and MISOMIP v. 1 (MISOMIP1), *Geoscientific Model Development*, *9*(7), 2471–2497, doi:10.5194/gmd-9-2471-2016. 6.2

Assmann, K. M., A. Jenkins, D. R. Shoosmith, D. P. Walker, S. S. Jacobs, and K. W. Nicholls (2013), Variability of circumpolar deep water transport onto the Amundsen Sea Continental shelf through a shelf break trough, *Journal of Geophysical Research: Oceans*, *118*(12), 6603–6620, doi:10.1002/2013JC008871. 2.2.3

Assmann, K. M., E. Darelius, A. Wåhlin, T. W. Kim, and S. H. Lee (2019), Warm Circumpolar Deep Water at the Western Getz Ice Shelf Front , Antarctica, *Geophysical Research Letters*, *46*(2), 870–878, doi:10.1029/2018GL081354. 2.1.3, 4.1

Bronselaer, B., M. Winton, S. M. Griffies, W. J. Hurlin, K. B. Rodgers, O. V. Sergienko, R. J. Stouffer, and J. L. Russell (2018), Change in future climate due to Antarctic meltwater, *Nature*, *564*(7734), 53–58, doi:10.1038/s41586-018-0712-z. 6.2

Chavanne, C. P., K. J. Heywood, K. W. Nicholls, and I. Fer (2010), Observations of the Antarctic Slope undercurrent in the Southeastern Weddell Sea, *Geophysical Research Letters*, *37*(13), 3–7, doi:10.1029/2010GL043603. 2.2.3

Christie, F. D., R. G. Bingham, N. Gourmelen, E. J. Steig, R. R. Bisset, H. D. Pritchard, K. Snow, and S. F. Tett (2018), Glacier change along West Antarctica's Marie Byrd Land Sector and links to inter-decadal atmosphere-ocean variability, *Cryosphere*, *12*(7), 2461–2479, doi:10.5194/tc-12-2461-2018. 2.1.3

Clem, K. R., J. A. Renwick, and J. Mcgregor (2017), Large-scale forcing of the Amundsen Sea low and its influence on sea ice and west antarctic temperature, *Journal of Climate*, *30*(20), 8405–8424, doi:10.1175/JCLI-D-16-0891.1. 2.1.2

Cushman-Roisin, B., and J.-M. Beckers (2011), *Introduction to Geophysical Fluid Dynamics: Physical and Numerical Aspects*, International Geophysical Series, second ed. 2.2.1, 2.2.2, 2.2.2

Dansereau, V., P. Heimback, and M. Losch (2013), Simulation of subice shelf melt rates in a general circulation model: Velocity-dependent transfer and the role of friction, *Journal of Geophysical Research: Oceans*, *119*, 17651790, doi:10.1002/2013JC008846.Received. 2.3.1

Darelius, E., I. Fer, K. Assmann, and T. W. Kim (2018), Physical oceanography from Mooring UiB1 and UiB4 in the Amundsen Sea, doi:https://doi.org/10.21335/NMDC-1721053841. **??**, **??**

Davis, P. E., A. Jenkins, K. W. Nicholls, P. V. Brennan, E. P. Abrahamsen, K. J. Heywood, P. Dutrieux, K. H. Cho, and T. W. Kim (2018), Variability in Basal Melting Beneath Pine Island Ice Shelf on Weekly to Monthly Timescales, *Journal of Geophysical Research: Oceans*, *123*(11), 8655–8669, doi:10.1029/2018JC014464. 2.2.4, 6.2, 6.2

Depoorter, M. A., J. L. Bamber, J. A. Griggs, J. T. Lenaerts, S. R. Ligtenberg, M. R. Van Den Broeke, and G. Moholdt (2013), Calving fluxes and basal melt rates of Antarctic ice shelves, *Nature*, *502*(7469), 89–92, doi:10.1038/nature12567. 2.1.3

Dinniman, M., X. Asay-Davis, B. Galton-Fenzi, P. Holland, A. Jenkins, and R. Timmermann (2016), Modeling ice shelf/ocean interaction in Antarctica: A review, *Oceanography*, *29*(4), 144–153, doi:https://doi.org/10.5670/oceanog.2016.106. 1

Dinniman, M. S., J. M. Klinck, and E. E. Hofmann (2012), Sensitivity of circumpolar deep water transport and ice shelf basal melt along the west antarctic peninsula to changes in the winds, *Journal of Climate*, *25*(14), 4799–4816, doi:10.1175/JCLI-D-11-00307.1. 6.2

Donat-Magnin, M., N. C. Jourdain, P. Spence, J. Le Sommer, H. Gallée, and G. Durand (2017), Ice-Shelf Melt Response to Changing Winds and Glacier Dynamics in the Amundsen Sea Sector, Antarctica, *Journal of Geophysical Research: Oceans*, *122*(12), 10,206–10,224, doi:10.1002/2017JC013059. 6.2

Dotto, T. S., A. C. Naveira Garabato, S. Bacon, P. R. Holland, S. Kimura, Y. L. Firing, M. Tsamados, A. K. Wåhlin, and A. Jenkins (2019), Wind-driven processes controlling oceanic heat delivery to the Amundsen Sea, Antarctica, *Journal of Physical Oceanography*, *49*(11), 2829–2849, doi:10.1175/jpo-d-19-0064.1. 6.2

Dotto, T. S., A. C. N. Garabato, A. K. Wåhlin, and S. Bacon (2020), Control of the Oceanic Heat Content of the Getz Dotson Trough , Antarctica , by the Amundsen Sea Low, *Journal of Geophysical Research : Oceans*, *125*(8), doi:10.1029/2020JC016113. 2.1.2, 2.2.3

Foldvik, A., T. Gammelsrød, E. Nygaard, and S. Østerhus (2001), Current measurements near Ronne Ice Shelf: Implications for circulation and melting, *Journal of Geophysical Research*, *106*(C3), 4463–4477. 2.2.4, 6.2

Fretwell, P., H. D. Pritchard, D. G. Vaughan, J. L. Bamber, N. E. Barrand, R. Bell, C. Bianchi, R. G. Bingham, D. D. Blankenship, G. Casassa, G. Catania, D. Callens, H. Conway, A. J. Cook, H. F. J. Corr, D. Damaske, V. Damm, F. Ferraccioli, R. Forsberg, S. Fujita, Y. Gim, P. Gogineni, J. A. Griggs, R. C. A. Hindmarsh, P. Holmlund, J. W. Holt, R. W. Jacobel, A. Jenkins, W. Jokat, T. Jordan, and E. King (2013), Bedmap2: improved ice bed, surface and thickness datasets for Antarctica, *The Cryosphere*, *7*, 375–393, doi:10.5194/tc-7-375-2013. 1

Fricker, H. A., S. Popov, I. Allison, and N. Young (2001), Distribution of marine ice beneath the Amery Ice Shelf, *Geophysical Research Letters*, *28*(11), 2241–2244. 2.3.1

Gao, M., S. J. Kim, J. Yang, J. Liu, T. Jiang, B. Su, Y. Wang, and J. Huang (2021), Historical fidelity and future change of Amundsen Sea Low under 1.5 °C4 °C global warming in CMIP6, *Atmospheric Research*, *255*(December 2020), 105,533, doi:10.1016/j.atmosres.2021.105533. 6.2

Garabato, A. C., A. Forryan, P. Dutrieux, L. Brannigan, L. C. Biddle, K. J. Heywood, A. Jenkins, Y. L. Firing, and S. Kimura (2017), Vigorous lateral export of the meltwater outflow from beneath an Antarctic ice shelf, *Nature*, *542*(7640), 219–222, doi:10.1038/nature20825. 2.3.1

Grosfeld, K., R. Gerdes, and J. Determann (1997), Thermohaline circulation and interaction between ice shelf cavities and the adjacent open ocean, *Journal of Geophysical Research C: Oceans*, *102*(C7), 15,595–15,610, doi:10.1029/97JC00891. 2.2.4, 4.4, 6.2

Ha, H. K., A. K. Wåhlin, T. W. Kim, S. H. Lee, J. H. Lee, H. J. Lee, C. S. Hong, L. Arneborg, G. Björk, and O. Kalén (2014), Circulation and Modification of Warm Deep Water on the Central Amundsen Shelf, *Journal of Physical Oceanography*, *44*(5), 1493–1501, doi:10.1175/JPO-D-13-0240.1. 2.3.1

Hattermann, T., O. A. Nst, J. M. Lilly, and L. H. Smedsrud (2012), Two years of oceanic observations below the Fimbul Ice Shelf, Antarctica, *Geophysical Research Letters*, *39*(12), doi:10.1029/2012GL051012. 2.3.2

Hersbach, H., B. Bell, P. Berrisford, G. Biavati, A. Horányi, J. Muñoz Sabater, J. Nicolas, C. Peubey, R. Radu, I. Rozum, D. Schepers, A. Simmons, C. Soci, D. Dee, and J.-N. Thépaut (2018), ERA5 hourly data on single levels from 1979 to present, *Copernicus Climate Change Service (C3S) Climate Data Store (CDS) (Accessed on 11-Sep-2020)*, doi:10.24381/cds.adbb2d47. 2.2, 4.2

Heywood, K., L. Biddle, L. Boehme, P. Dutrieux, M. Fedak, A. Jenkins, R. Jones, J. Kaiser, H. Mallett, A. N. Garabato, I. Renfrew, D. Stevens, and B. Webber (2016), Between the devil and the deep blue sea: The role of the Amundsen Sea continental shelf in exchanges between ocean and ice shelves, *Oceanography*, *29*(4), 118129, doi:https://doi.org/10.5670/oceanog.2016.104. 2.1.1

Heywood, K. J., A. C. Naveira Garabato, D. P. Stevens, and R. D. Muench (2004), On the fate of the Antarctic Slope Front and the origin of the Weddell Front, *Journal of Geophysical Research C: Oceans*, *109*(6), 1–13, doi:10.1029/2003JC002053. 2.2.3

Hobbs, W. R., R. Massom, S. Stammerjohn, P. Reid, G. Williams, and W. Meier (2016), A review of recent changes in Southern Ocean sea ice, their drivers and forcings, *Global and Planetary Change*, *143*, 228–250, doi:10.1016/j.gloplacha.2016.06.008. 2.1.2

Holland, D. M., K. W. Nicholls, and A. Basinski (2020), The Southern Ocean and its interaction with the Antarctic Ice Sheet, *Science*, *367*(6484), 1326–1330, doi:10.1126/science.aaz5491. 1

Holland, P. R., and R. Kwok (2012), Wind-driven trends in Antarctic sea-ice drift, *Nature Geoscience*, *5*(12), 872–875, doi:10.1038/ngeo1627. 2.1.2

Holland, P. R., A. Jenkins, and D. M. Holland (2008), The response of Ice shelf basal melting to variations in ocean temperature, *Journal of Climate*, *21*(11), 2558–2572, doi:10.1175/2007JCLI1909.1. 2.3.1, 2.3.2

Hughes, C. W., I. Fukumori, S. M. Griffies, J. M. Huthnance, S. Minobe, P. Spence, K. R. Thompson, and A. Wise (2019), Sea Level and the Role of Coastal Trapped Waves in Mediating the Influence of the Open

Ocean on the Coast, *Surveys in Geophysics*, *40*(6), 1467–1492, doi:10.1007/s10712-019-09535-x. 2.2.1

Hughes, T. (1973), Is the west Antarctic Ice Sheet disintegrating?, *Journal of Geophysical Research*, *78*(33), 7884–7910, doi:10.1029/jc078i033p07884. 2.3.1

Jacobs, S. S. (1991), On the nature and significance of the Antarctic Slope Front, *Marine Chemistry*, *35*(1-4), 9–24, doi:10.1016/S0304-4203(09)90005-6. 2.2.3

Jacobs, S. S., H. H. Helmer, C. S. Doake, A. Jenkins, and R. M. Frolich (1992), Melting of ice shelves and the mass balance of Antarctica, *Journal of Glaciology*, *38*(130), 375–387, doi:10.1017/S0022143000002252. 1, 2.3.2, 2.4

Jacobs, S. S., H. H. Hellmer, and A. Jenkins (1996), Antarctic Ice Sheet melting in the southeast Pacific, *Geophysical Research Letters*, *23*(9), 957–960, doi:10.1029/96GL00723. 2.1.1

Jacobs, S. S., C. F. Giulivi, and P. A. Mele (2002), Freshening of the Ross Sea during the late 20th century, *Science*, *297*(5580), 386–389, doi:10.1126/science.1069574. 2.1.3

Jacobs, S. S., A. Jenkins, H. Hellmer, C. Giulivi, F. Nitsche, B. Huber, and R. Guerrero (2012), The Amundsen Sea and the Antarctic Ice Sheet, *Oceanography*, *25*(3), 154–163, doi:10.5670/oceanog.2012.90. 2.1.1, 2.1.3

Jacobs, S. S., C. F. Giulivi, P. Dutrieux, E. Rignot, F. Nitsche, and J. Mouginot (2013), Getz Ice Shelf melting response to changes in ocean forcing, *Journal of Geophysical Research: Oceans*, *118*(9), 4152–4168, doi:10.1002/jgrc.20298. 2.1.3

Jenkins, A. (1991), A One-Dimensional Model of Ice Shelf-Ocean Interaction, *Journal of Geophysical Research*, *96*(Cll), 20,671–20,677, doi:10.1029/91JC01842. 2.4

Jenkins, A. (2011), Convection-driven melting near the grounding lines of ice shelves and tidewater glaciers, *Journal of Physical Oceanography*, *41*(12), 2279–2294, doi:10.1175/JPO-D-11-03.1. 2.3.1

Jenkins, A., S. Jacobs, and J. Keys (1994), Is this little PIG in hot water, *Antarctic Journal of the United States*, *29*(5), 121–122. 2.1.1

Jenkins, A., P. Dutrieux, S. S. Jacobs, S. D. McPhail, J. R. Perrett, A. T. Webb, and D. White (2010), Observations beneath Pine Island Glacier in West-Antarctica and implications for its retreat, *Nature Geoscience*, *3*(7), 468–472, doi:10.1038/ngeo890. 2.3.1

Jenkins, A., P. Dutrieux, S. Jacobs, E. J. Steig, G. H. Gudmundsson, and J. Smith (2016), Decadal ocean forcing and Antarctic ice sheet response: Lessons from the Amundsen Sea, *Oceanography*, *29*(4), 106117, doi:https://doi.org/10.5670/oceanog.2016.103. 1, 2.1.1

Joughin, I., and R. B. Alley (2011), Stability of the West Antarctic ice sheet in a warming world, *Nature Publishing Group*, *4*(8), 506–513, doi:10.1038/ngeo1194. 1

Jourdain, N. C., P. Mathiot, N. Merino, G. Durand, J. Le Sommer, P. Spence, P. Dutrieux, and G. Madec (2017), Ocean circulation and sea-ice thinning induced by melting ice shelves in the Amundsen Sea, *Journal of Geophysical Research: Oceans*, *122*(3), 2550–2573, doi:10.1002/2016JC012509. 2.1.3, 2.3.1

Jourdain, N. C., J. M. Molines, J. Le Sommer, P. Mathiot, J. Chanut, C. de Lavergne, and G. Madec (2019), Simulating or prescribing the influence of tides on the Amundsen Sea ice shelves, *Ocean Modelling*, *133*(October 2018), 44–55, doi:10.1016/j.ocemod.2018.11.001. 2.2.4

Kalén, O., K. M. Assmann, A. K. Wåhlin, H. K. Ha, T. W. Kim, and S. H. Lee (2016), Is the oceanic heat flux on the central Amundsen sea shelf caused by barotropic or baroclinic currents?, *Deep-Sea Research Part II: Topical Studies in Oceanography*, *123*, 7–15, doi:10.1016/j.dsr2.2015.07.014. 2.2.1, 2.3.1

Karam, S. (2019), Variability in basal melting beneath Getz Ice Shelf on tidal to seasonal time scales, *Master Thesis*. 6.2

Kim, C. S., T. W. Kim, K. H. Cho, H. K. Ha, S. H. Lee, H. C. Kim, and J. H. Lee (2016), Variability of the Antarctic Coastal Current in the Amundsen Sea, *Estuarine, Coastal and Shelf Science*, *181*, 123–133, doi:10.1016/j.ecss.2016.08.004. 2.2.4, 6.2

Kimura, S., A. S. Candy, P. R. Holland, M. D. Piggott, and A. Jenkins (2013), Adaptation of an unstructured-mesh, finite-element ocean model to the simulation of ocean circulation beneath ice shelves, *Ocean Modelling*, *67*, 39–51, doi:10.1016/j.ocemod.2013.03.004. 1

Kimura, S., A. Jenkins, H. Regan, P. R. Holland, K. M. Assmann, D. B. Whitt, M. Van Wessem, W. J. van de Berg, C. H. Reijmer, and P. Dutrieux (2017), Oceanographic Controls on the Variability of Ice-Shelf Basal Melting and Circulation of Glacial Meltwater in the Amundsen Sea Embayment, Antarctica, *Journal of Geophysical Research: Oceans*, *122*(12), 10,131–10,155, doi:10.1002/2017JC012926. 2.3.1

Konrad, H., A. Shepherd, L. Gilbert, A. E. Hogg, M. McMillan, A. Muir, and T. Slater (2018), Net retreat of Antarctic glacier grounding lines, *Nature Geoscience*, *11*(4), 258–262, doi:10.1038/s41561-018-0082-z. 6.2

Lewis, E. L., and R. G. Perkin (1986), Ice pumps and their rates, *Journal of Geophysical Research*, *91*(C10), 11,756, doi:10.1029/jc091ic10p11756. 2.3.1

Little, C. M., A. Gnanadesikan, and M. Oppenheimer (2009), How ice shelf morphology controls basal melting, *Journal of Geophysical Research: Oceans*, *114*(12), doi:10.1029/2008JC005197. 2.3.1

Liu, Y., J. C. Moore, X. Cheng, R. M. Gladstone, J. N. Bassis, H. Liu, J. Wen, and F. Hui (2015), Ocean-driven thinning enhances iceberg calving and retreat of Antarctic ice shelves, *Proceedings of the National Academy of Sciences of the United States of America*, *112*(11), 3263–3268, doi:10.1073/pnas.1415137112. 2.3.1

Losch, M. (2008), Modeling ice shelf cavities in a z coordinate ocean general circulation model, *Journal of Geophysical Research: Oceans*, *113*(8), 1–15, doi:10.1029/2007JC004368. 1, 4.4

Makinson, K., and K. W. Nicholls (1999), Modeling tidal currents beneath Filchner-Ronne Ice Shelf and on the adjacent continental shelf: Their effect on mixing and transport, *Journal of Geophysical Research: Oceans*, *104*(C6), 13,449–13,465, doi:10.1029/1999jc900008. 2.2.4

Mankoff, K. D., S. S. Jacobs, S. M. Tulaczyk, and S. E. Stammerjohn (2012), The role of pine island glacier ice shelf basal channels in deep-water upwelling, polynyas and ocean circulation in pine island bay, antarctica, *Annals of Glaciology*, *53*(60), 123–128, doi:10.3189/2012AoG60A062. 2.3.1

Marshall, G. J. (2003), Trends in the Southern Annular Mode from observations and reanalyses, *Journal of Climate*, *16*(24), 4134–4143, doi:10.1175/1520-0442(2003)016<4134:TITSAM>2.0.CO;2. 2.1.2, 6.2

Marshall, J., A. Adcroft, C. Hill, L. Perelman, and C. Heisey (1997a), A finite-volume, incompressible navier stokes model for, studies of the ocean on parallel computers, *Journal of Geophysical Research C: Oceans*, *102*(C3), 5753–5766, doi:10.1029/96JC02775. 4.4

Marshall, J., C. Hill, L. Perelman, and A. Adcroft (1997b), Hydrostatic, quasi-hydrostatic, and nonhydrostatic ocean modeling, *Journal of Geophysical Research C: Oceans*, *102*(C3), 5733–5752, doi:10.1029/96JC02776. 4.4

Mazur, A. K., A. K. Wåhlin, and A. Krężel (2017), An object-based SAR image iceberg detection algorithm applied to the Amundsen Sea, *Remote Sensing of Environment*, *189*, 67–83, doi:10.1016/j.rse.2016.11.013. 2.1.2

McKee, D. C., and D. G. Martinson (2020), Wind-Driven Barotropic Velocity Dynamics on an Antarctic Shelf, *Journal of Geophysical Research: Oceans*, *125*(5), 1–21, doi:10.1029/2019JC015771. 2.1.2

Millgate, T., P. R. Holland, A. Jenkins, and H. L. Johnson (2013), The effect of basal channels on oceanic ice-shelf melting, *Journal of Geophysical Research: Oceans*, *118*(12), 6951–6964, doi:10.1002/2013JC009402. 2.3.1

Nakayama, Y., R. Timmermann, C. B. Rodehacke, M. Schröder, and H. H. Hellmer (2014), Modeling the spreading of glacial meltwater from the Amundsen and Bellingshausen Seas, *Geophysical Research Letters*, *41*(22), 7942–7949, doi:10.1002/2014GL061600. 2.1.3, 2.3.1

Nakayama, Y., D. Menemenlis, H. Zhang, M. Schodlok, and E. Rignot (2018), Origin of Circumpolar Deep Water intruding onto the Amundsen and Bellingshausen Sea continental shelves, *Nature Communications*, *9*(1), 1–9, doi:10.1038/s41467-018-05813-1. 6.2

Nicholls, K. W. (1996), Temperature variability beneath Ronne Ice Shelf, Antarctica, from thermistor cables, *Journal of Geophysical Research C: Oceans*, *101*(C1), 1199–1210, doi:10.1029/95JC02679. 2.3.1

Nicholls, K. W., L. Padman, M. Schröder, R. Woodgate, A. Jenkins, and S. Østerhus (2003), Water mass modification over the continental shelf north of Ronne Ice Shelf, Antarctica, *Journal of Geophysical Research*, *108*(C8), 3260, doi:10.1029/2002JC001713. 2.2.4

Orsi, A. H., T. Whitworth, and W. D. Nowlin (1995), On the meridional extent and fronts of the Antarctic Circumpolar Current Pronounced meridional gradients in surface properties separate waters of the Southern Ocean from the warmer and saltier waters of the subtropical circulations . Deacon (1933 , the S, *Deep-Sea Research Part I: Oceanographic Research Papers*, *42*(5), 641 – 673, doi:https://doi.org/10.1016/0967-0637(95)00021-W. 1, 2.1.1, 2.2.3

Padman, L., D. P. Costa, M. S. Dinniman, H. A. Fricker, M. E. Goebel, L. A. Huckstadt, A. Humbert, I. Joughin, J. T. Lenaerts, S. R. Ligtenberg, T. Scambos, and M. R. Van Den Broeke (2012), Oceanic controls on the mass balance of Wilkins Ice Shelf, Antarctica, *Journal of Geophysical Research: Oceans*, *117*(1), 1–17, doi:10.1029/2011JC007301. 6.2

Padman, L., M. R. Siegfried, and H. A. Fricker (2018), Ocean Tide Influences on the Antarctic and Greenland Ice Sheets, *Reviews of Geophysics*, *56*(1), 142–184, doi:10.1002/2016RG000546. 2.2.1, 2.2.4, 6.2

Palóczy, A., S. T. Gille, and J. L. McClean (2018), Oceanic Heat Delivery to the Antarctic Continental Shelf: Large-Scale, Low-Frequency Variability, *Journal of Geophysical Research: Oceans*, *123*(11), 7678–7701, doi:10.1029/2018JC014345. 2.2.3

Paolo, F. S., H. A. Fricker, and L. Padman (2015), Volume loss from Antarctic ice shelves is accelerating, *Science*, *348*(6232), 327–332, doi:10.1017/CBO9781107415324.004. 1, 2.1.3

Paolo, F. S., L. Padman, H. A. Fricker, S. Adusumilli, S. Howard, and M. R. Siegfried (2018), Response of Pacific-sector Antarctic ice shelves to the El Niño/Southern Oscillation, *Nature Geoscience*, *11*(2), 121–126, doi:10.1038/s41561-017-0033-0. 2.1.2

Parkinson, C. L. (2019), A 40-y record reveals gradual Antarctic sea ice increases followed by decreases at rates far exceeding the rates seen in the Arctic, *Proceedings of the National Academy of Sciences of the United States of America*, *116*(29), 14,414–14,423, doi:10.1073/pnas.1906556116. 6.2

Pattyn, F., and M. Morlighem (2020), The Uncertain Future of the West Antarctic Ice Sheet, *Science*, *367*, 1331–1335, doi:10.1029/2018eo074147. 1, 6.2

Pritchard, H., S. Ligtenberg, H. Fricker, D. Vaughan, M. van den Broeke, and L. Padman (2012), Antarctic ice-sheet loss driven by basal melting of ice shelves, *Nature*, *484*(7395), 502–505, doi:10.1038/nature10968. 1, 2.1.1

Pritchard, H. D., R. J. Arthern, D. G. Vaughan, and L. A. Edwards (2009), Extensive dynamic thinning on the margins of the Greenland and Antarctic ice sheets., *Nature*, *461*(7266), 971–975, doi:10.1038/nature08471. 2.1.3

Raphael, M. N., G. J. Marshall, J. Turner, R. L. Fogt, D. Schneider, D. A. Dixon, J. S. Hosking, J. M. Jones, and W. R. Hobbs (2016), The Amundsen sea low: Variability, change, and impact on Antarctic climate, *Bulletin of the American Meteorological Society*, *97*(1), 111–121, doi:10.1175/BAMS-D-14-00018.1. 2.1.2

Reese, R., G. H. Gudmundsson, A. Levermann, and R. Winkelmann (2018), The far reach of ice-shelf thinning in Antarctica, *Nature Climate Change*, *8*(1), 53–57, doi:10.1038/s41558-017-0020-x. 1, 2.1.3

Rignot, E., S. Jacobs, J. Mouginot, and B. Scheuchl (2013), Ice-Shelf Melting Around Antarctica, *Science*, *341*(6143), 266–270, doi:10.1126/science.1235798. 1

Rignot, E., J. Mouginot, M. Morlighem, H. Seroussi, and B. Scheuchl (2014), Widespread, rapid grounding line retreat of Pine Island, Thwaites, Smith, and Kohler glaciers, West Antarctica, from 1992 to 2011, *Geophysical Research Letters*, *41*(10), 3502–3509, doi:10.1002/2014GL060140. 1

Rintoul, S. R., M. Sparrow, M. P. Meredith, V. Wadley, K. Speer, E. Hofmann, C. Summerhayes, E. Urban, and R. Bellerby (2012), *The Southern Ocean Observing System: Initial Science and Implementation Strategy*, 74 pp. 1

Robertson, R. (2005), Baroclinic and barotropic tides in the Weddell Sea, *Antarctic Science*, *17*(3), 461–474, doi:10.1017/S0954102005002890. 2.2.1, 2.2.4

Robertson, R. (2013), Tidally induced increases in melting of Amundsen Sea ice shelves, *Journal of Geophysical Research: Oceans*, *118*(6), 3138–3145, doi:10.1002/jgrc.20236. 2.2.4

Schaffer, J., R. Timmermann, J. Erik Arndt, S. Savstrup Kristensen, C. Mayer, M. Morlighem, and D. Steinhage (2016), A global, high-resolution data set of ice sheet topography, cavity geometry, and ocean bathymetry, *Earth System Science Data*, *8*(2), 543–557, doi:10.5194/essd-8-543-2016. 4.1

Schoof, C. (2007), Ice sheet grounding line dynamics: Steady states, stability, and hysteresis, *Journal of Geophysical Research: Earth Surface*, *112*(3), 1–19, doi:10.1029/2006JF000664. 1, 6.2

Selley, H. L., A. E. Hogg, S. Cornford, P. Dutrieux, A. Shepherd, J. Wuite, D. Floricioiu, A. Kusk, T. Nagler, L. Gilbert, T. Slater, and T. W. Kim (2021), Widespread increase in dynamic imbalance in the Getz region of Antarctica from 1994 to 2018, *Nature Communications*, *12*(1), 1–10, doi:10.1038/s41467-021-21321-1. 2.1.3

Shepherd, A., H. A. Fricker, and S. L. Farrell (2018), Trends and connections across the Antarctic cryosphere, *Nature*, *558*(7709), 223–232, doi:10.1038/s41586-018-0171-6. 1, 2.1.1, 2.1, 2.1.3, 6.2

Shepherd, A., L. Gilbert, A. S. Muir, H. Konrad, M. McMillan, T. Slater, K. H. Briggs, A. V. Sundal, A. E. Hogg, and M. E. Engdahl (2019), Trends in Antarctic Ice Sheet Elevation and Mass, *Geophysical Research Letters*, *46*(14), 8174–8183, doi:10.1029/2019GL082182. 2.1.3

Silvano, A., S. R. Rintoul, B. Peña-Molino, W. R. Hobbs, E. van Wijk, S. Aoki, T. Tamura, and G. D. Williams (2018), Freshening by glacial meltwater enhances melting of ice shelves and reduces formation of Antarctic Bottom Water, *Science Advances*, *4*(4), eaap9467, doi:10.1126/sciadv.aap9467. 2.1.3

Spence, P., S. M. Griffies, M. H. England, A. M. C. Hogg, O. A. Saenko, and N. C. Jourdain (2014), Rapid subsurface warming and circulation changes of Antarctic coastal waters by poleward shifting winds, *Geophysical Research Letters*, *41*(13), 4601–4610, doi:10.1002/2014GL060613.Received. 6.2

Spence, P., R. M. Holmes, A. M. Hogg, S. M. Gri, K. D. Stewart, and M. H. England (2017), Localized rapid warming of West Antarctic subsurface waters by remote winds, *Nature Climate Change*, *7*, 595–604, doi:10.1038/NCLIMATE3335. 2.2.1, 6.2

Spreen, G., L. Kaleschke, and G. Heygster (2008), Sea ice remote sensing using AMSR-E 89-GHz channels, *Journal of Geophysical Research: Oceans*, *113*(2), 1–14, doi:10.1029/2005JC003384. 2.2, 4.2

St-Laurent, P., J. M. Klinck, and M. S. Dinniman (2013), On the Role of Coastal Troughs in the Circulation of Warm Circumpolar Deep Water on Antarctic Shelves, *Journal of Physical Oceanography*, *43*(1), 51–64, doi:10.1175/JPO-D-11-0237.1. 1, 2.2.3

St-Laurent, P., J. Klinck, and M. Dinniman (2015), Impact of local winter cooling on the melt of Pine Island Glacier, Antarctica, *Journal of Geophysical Research: Oceans*, *120*(10), 6718–6732, doi:10.1002/2015JC010709. 2.2.4, 6.2, 6.2

Stewart, A. L., A. Klocker, and D. Menemenlis (2018), Circum-Antarctic Shoreward Heat Transport Derived From an Eddy- and Tide-Resolving Simulation, *Geophysical Research Letters*, *45*(2), 834–845, doi:10.1002/2017GL075677. 2.2.3

Stewart, C. L., P. Christoffersen, K. W. Nicholls, M. J. Williams, and J. A. Dowdeswell (2019), Basal melting of Ross Ice Shelf from solar heat absorption in an ice-front polynya, *Nature Geoscience*, *12*(6), 435–440, doi:10.1038/s41561-019-0356-0. 2.2.4

Stewart, R. H. (2008), *Introduction To Physical Oceanography*, September. 2.2.2

Stocker, T., Q. Qin, G.-K. Plattner, M. Tignor, S. Allen, J. Boschung, A. Nauels, Y. Xia, B. V., M. P.M., and (eds.) (2013), *Climate Change 2013: The Physical Science Basis. Contribution of Working Group I to the Fifth Assessment Report of the Intergovernmental Panel on Climate Change*, 1535 pp., Cambridge University Press, Cambridge, United Kingdom and New York, NY, USA. 1

Sverdrup, H. (1953), The currents off the coast of Queen Maud Land, *Norsk Geografisk Tidsskrift-Norwegian J. Geogr.*, *14*(1-4), 239e249. 2.2.3

Thoma, M., A. Jenkins, D. Holland, and S. Jacobs (2008), Modelling Circumpolar Deep Water intrusions on the Amundsen Sea continental shelf, Antarctica, *Geophysical Research Letters*, *35*(18), 2–7, doi:10.1029/2008GL034939. 1, 2.1.2, 2.2.3

Thomas, R. H. (1979), The Dynamics of Marine Ice Sheets, *Journal of Glaciology*, *24*(90), 167 – 177. 1

Thompson, A. F., K. J. Heywood, S. Schmidtko, and A. L. Stewart (2014), Eddy transport as a key component of the Antarctic overturning circulation, *Nature Geoscience*, *7*(12), 879–884, doi:10.1038/ngeo2289. 2.2.3

Thompson, A. F., A. L. Stewart, P. Spence, and K. J. Heywood (2018), The Antarctic Slope Current in a Changing Climate, *Reviews of Geophysics*, pp. 1–41, doi:10.1029/2018RG000624. 2.2.3

Thompson, D. W., and J. M. Wallace (2000), Annular modes in the extratropical circulation. Part I: Month-to-month variability, *Journal of Climate*, *13*(5), 1000–1016, doi:10.1175/1520-0442(2000)013<1000:AMITEC>2.0.CO;2. 2.2.1

Turner, J., T. Phillips, J. S. Hosking, G. J. Marshall, and A. Orr (2013), The amundsen sea low, *International Journal of Climatology*, *33*(7), 1818–1829, doi:10.1002/joc.3558. 2.1.2

Vivier, F., K. A. Kelly, and M. Harismendy (2005), Causes of large-scale sea level variations in the Southern Ocean: Analyses of sea level and a barotropic model, *Journal of Geophysical Research C: Oceans*, *110*(9), 1–20, doi:10.1029/2004JC002773. 2.2.1

Wåhlin, A. K. (2002), Topographic steering of dense currents with application to submarine canyons, *Deep-Sea Research Part I: Oceanographic Research Papers*, *49*(2), 305–320, doi:10.1016/S0967-0637(01)00058-9. 6.2

Wåhlin, A. K. (2004), Topographic advection of dense bottom water, *Journal of Fluid Mechanics*, *510*, 95–104, doi:10.1017/S0022112004009590. 6.2

Wåhlin, A. K., R. D. Muench, L. Arneborg, G. Björk, H. K. Ha, S. H. Lee, and H. Alsén (2012), Some implications of ekman layer dynamics for cross-shelf exchange in the Amundsen sea, *Journal of Physical Oceanography*, *42*(9), 1461–1474, doi:10.1175/JPO-D-11-041.1. 2.2.3

Wåhlin, A. K., O. Kalén, L. Arneborg, G. Björk, G. K. Carvajal, H. K. Ha, T. W. Kim, S. H. Lee, J. H. Lee, and C. Stranne (2013), Variability of Warm Deep Water Inflow in a Submarine Trough on the Amundsen Sea Shelf, *Journal of Physical Oceanography*, *43*, 2054–2070, doi:10.1175/JPO-D-12-0157.1. 2.1.3, 2.2.1, 2.2.3

Wåhlin, A. K., O. Kalén, K. M. Assmann, E. Darelius, H. K. Ha, T.-W. Kim, and S. H. Lee (2016), Subinertial Oscillations on the Amundsen Sea Shelf, Antarctica, *Journal of Physical Oceanography*, *46*(9), 2573–2582, doi:10.1175/jpo-d-14-0257.1. 2.2.1

Wåhlin, A. K., J. Rolandsson, and K. Assmann (2019), Horizontal components of current velocity collected by ADCP from a mooring deployed and recovered by research vessel ice breaker Araon in the Amundsen Sea from 2016-01-28 to 2018-01-18, *NOAA National Centers for Environmental Information*, doi:https://doi.org/10.25921/n07g-f935. **??**

Wåhlin, A. K., N. Steiger, E. Darelius, K. M. Assmann, M. S. Glessmer, H. K. Ha, A. Jenkins, T. W. Kim, A. K. Mazur, J. Sommeria, and S. Viboud (2020), Ice front blocking of ocean heat transport to an Antarctic ice shelf, *Nature*, *578*, 568–571, doi:10.1038/s41586-020-2014-5. 2.3, 4.3

Wåhlin, J. A. K., A.K.; Rolandsson (2019), Water temperature, salinity, oxygen, and other oceanographic data collected by CTD from a mooring deployed and recovered by the research vessel ice breaker Araon in the Amundsen Sea from 2016-01-28 to 2018-01-18, *NOAA National Centers for Environmental Information*, doi:https://doi.org/10.25921/6pwp-1791. **??**

Walker, D. P., M. A. Brandon, A. Jenkins, J. T. Allen, J. A. Dowdeswell, and J. Evans (2007), Oceanic heat transport onto the Amundsen Sea shelf through a submarine glacial trough, *Geophysical Research Letters*, *34*(2), 2–5, doi:10.1029/2006GL028154. 1, 2.2.3

Walker, D. P., A. Jenkins, K. M. Assmann, D. R. Shoosmith, and M. A. Brandon (2013), Oceanographic observations at the shelf break of the Amundsen Sea, Antarctica, *Journal of Geophysical Research: Oceans*, *118*(6), 2906–2918, doi:10.1002/jgrc.20212. 2.2.3

Webb, D. J., R. M. Holmes, P. Spence, and M. H. England (2019), Barotropic Kelvin Wave-Induced Bottom Boundary Layer Warming Along the West Antarctic Peninsula, *Journal of Geophysical Research: Oceans*, *124*(3), 1595–1615, doi:10.1029/2018JC014227. 2.2.1

Webber, B. G., K. J. Heywood, D. P. Stevens, P. Dutrieux, E. P. Abrahamsen, A. Jenkins, S. S. Jacobs, H. K. Ha, S. H. Lee, and T. W. Kim (2017), Mechanisms driving variability in the ocean forcing of Pine Island Glacier, *Nature Communications*, *8*, 1–8, doi:10.1038/ncomms14507. 2.2.4, 6.2

Williams, W. J., G. G. Gawarkiewicz, and R. C. Beardsley (2001), The adjustment of a shelfbreak jet to cross-shelf topography, *Deep-Sea Research Part II:*

Topical Studies in Oceanography, *48*(1-3), 373–393, doi:10.1016/S0967-0645(00)00085-0. 2.3.1

Graphic design: Communication Division, UiB / Print: Skipnes Kommunikasjon AS

uib.no

ISBN: 9788230857403 (print)
9788230844588 (PDF)